Combined Effects of Soil Stress History and Scour Hole Dimensions on Laterally and Axially Loaded Piles in Sand and Clay under Scour Conditions

Yijian Zhang, Ph.D., P.E., M.ASCE[1]; and Iris Tien, Ph.D., M.ASCE[2]

Abstract: Removal of soil around a bridge foundation due to scour results in a reduction of the lateral and vertical foundation capacity due to the loss of soil support. The common approach in modeling the scour phenomenon of removal of soil springs without modifying the parameters of the remaining soil fails to consider the change of stress state of the remaining soil and the formation of scour hole geometry around the pile foundation. In practice, both of these factors impact the mechanical properties of the remaining soil and the resulting expected structural response of the pile under loadings. This paper proposed a methodology to comprehensively evaluate the combined effects of stress history and scour hole dimensions on piles under scour conditions in uniform soil. It enabled the examination of the lateral and axial behaviors of a loaded pile subject to scour and is applicable for both cohesive and cohesionless soils. The methodology was validated with results from field tests for no-scour scenarios and verified with existing numerical models for scour scenarios. Quantification of the soil effects was investigated through lateral pile deflection and load-settlement curves for lateral and axial behaviors, respectively. Load-settlement curves demonstrated that including the effect of stress history results in increases of up to 34.1% and 61.1% in estimated pile settlement for sand and clay, respectively, leading to potential unconservative designs if soil effects are not properly included in the analysis. **DOI: 10.1061/(ASCE)GT.1943-5606.0002786.**

Author keywords: Soil stress history; Scour hole dimensions; Scour; Laterally loaded piles; Axially loaded piles; Soil–structure interaction; Sand; Clay.

Introduction

Bridges built over flowing water are often susceptible to scour with the removal of material in the streambed or bank around bridge foundations. The erosion or removal of soil reduces bridge capacity from the loss of both lateral and vertical support to the structure, increasing the risk of bridge failures. Studies have estimated that approximately 60% of bridge failures are caused by scour-related issues (Lagasse et al. 2007). Hence, it is crucial to have an approach to accurately capture soil–structure interaction in the modeling of bridges under scour conditions. In recent years, Qi et al. (2016) have studied the effects of scour on *p-y* curves for shallowly embedded piles in sand. Wang et al. (2017) presented both an experimental study and numerical simulation to investigate the performance of sacrificial piles in reducing local scour round pile groups. Lin and Lin (2020) demonstrated the scour effects on lateral behavior of pile groups in sands. Liang et al. (2020) performed a series of centrifuge tests on a reinforced concrete bridge with a 3×3 pile-group foundation to study the seismic response under various scour conditions. Zhang et al. (2021) investigated the dynamic impedances of scoured monopoles for wind turbines, considering both scour hole geometries and soil stress history.

Among the existing literature, however, only limited studies have investigated the combined effects of stress history and scour hole dimensions on the structural behavior of foundation piles or bridges in the presence of scour. None have provided a comprehensive approach to this topic to enable a way to investigate both lateral and axial pile behavior under scour in cohesive and cohesionless soils, accounting for stress history and scour hole dimension effects. The following studies encapsulated the state-of-the-art soil–structure modeling approaches used to capture soil effects in the presence of scour.

For studies regarding the impact of soil stress history, Lin et al. (2010, 2014b) investigated the effect of stress history on lateral behavior of piles under scour conditions in sand and soft clay, respectively. Liang et al. (2015) performed a buckling analysis of bridge piles in the presence of scour, considering the impact of stress history in soft clay. Zhang and Tien (2020) presented a methodology to account for the impact of stress history in layered soils in the risk assessment of scoured bridges. For studies regarding the impact of scour hole dimensions, Lin et al. (2014a, 2016) proposed a simplified method to account for the effect of scour hole geometries on laterally loaded piles through an equivalent wedge failure model in sand and soft clay, respectively. Later, Lin (2017) studied the loss of pile axial capacities in the presence of scour considering scour hole dimensions based on Boussinesq's theory. Zhang et al. (2016) and Liang et al. (2018) investigated the combined effect of soil stress history and scour hole geometries on the lateral performance of piles in clay. Recently, Lin and Jiang (2019) compared the suitability of existing methods [i.e., Federal Highway Administration (FHWA) and American Petroleum Institute (API)] and the proposed analytical solution for estimating pile tension capacity using finite-element analyses under different scour hole dimensions. Jiang et al. (2021) proposed a new method to evaluate the postscour seismic responses of monopole-supported offshore wind turbines, considering various

[1]Research Affiliate, School of Civil and Environmental Engineering, Georgia Institute of Technology, Atlanta, GA 30332-0355 (corresponding author). Email: zyj.albert@gatech.edu

[2]Associate Professor, School of Civil and Environmental Engineering, Georgia Institute of Technology, Atlanta, GA 30332-0355. ORCID: https://orcid.org/0000-0002-1410-632X

Note. This manuscript was submitted on April 21, 2021; approved on January 6, 2022; published online on March 12, 2022. Discussion period open until August 12, 2022; separate discussions must be submitted for individual papers. This paper is part of the ***Journal of Geotechnical and Geoenvironmental Engineering***, © ASCE, ISSN 1090-0241.

dimensions and soil stress history changes due to different scour levels.

Among the aforementioned literature, a comprehensive approach to account for the combined effect of stress history and scour hole dimensions for both clay and sand on the behavior of foundation piles is lacking. In particular, existing studies focused on the impact of the soil effect on the lateral performance of piles while ignoring the impact on the axial performance (i.e., settlement) of the piles in the presence of scour. This paper presents a methodology to combine the effects of soil stress history and scour hole dimensions to more comprehensively model soil–structure interaction in both sand and clay. The study assumed piles in uniform soil, exploring the most vulnerable scenario for piles in uniform soil under scour effects. The combined effect of scour was captured through updating the parameters of the nonlinear soil springs (e.g., *p*-*y*, *t*-*z*, and *q*-*z* springs) in both the lateral and vertical directions. For the first time, comprehensive verification of the proposed generalized approach for modeling laterally and axially loaded piles in sand and clay subject to scour is provided.

The rest of the paper is structured as follows. The next section introduces background on the effects of soil stress history and scour hole dimensions for both sand and clay. The proposed methodology that combines these two soil effects is then presented. Derivations of the relationships updating the soil parameters in the presence of scour are provided. The following section provides validations/verifications and multiple analyses of laterally and axially loaded piles with and without considering soil effects in sand and clay. The proposed method was validated through comparing the pile deflection response using the proposed approach with measured results from field tests and verified with existing numerical models considering either individual or combined soil effects under scour scenarios. Analyses showed the impacts of including soil effects in estimated pile responses. The last part of this section demonstrates the ability of the proposed method to capture the combined soil effect with load-settlement curves in the presence of scour, showing the importance of including these soil effects in the estimation of structural responses under scour.

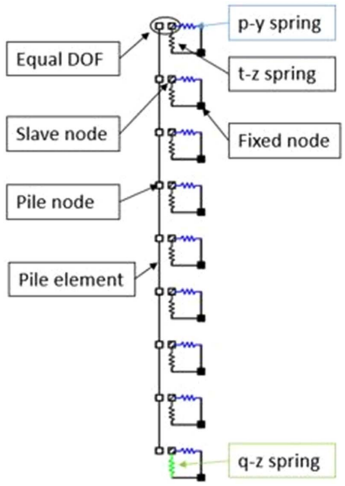

Fig. 1. Modeling of soil–structure interaction soil springs.

Table 1. Nonlinear backbone curves for sand and clay

	References	
Soil parameters	Sand	Clay
p-*y* curve	API (2000)	Matlock (1970)
Ultimate lateral resistance, P_{ult}	Reese et al. (1974)	Matlock (1970)
t-*z* curve	Mosher (1984)	Reese and O'Neill (1987)
Ultimate unit shaft resistance, T_{ult}	Tuma and Reese (1974)	Tomlinson and Boorman (2001)
q-*z* curve	Vijayvergiya (1977)	Reese and O'Neill (1987)
Ultimate bearing resistance, Q_{ult}	Meyerhof (1976)	Terzaghi (1943)

Background

Soil–Structure Interaction Model

To conduct nonlinear time history analyses and explicitly account for soil–structure interaction within tractable computing times, a dynamic beam on a nonlinear Winkler foundation or dynamic *p*-*y* method was adopted (Boulanger et al. 1999; Wang et al. 2014). The soil–structure interaction was modeled via three nonlinear springs (i.e., *p*-*y*, *t*-*z*, and *q*-*z* springs) to simulate lateral, frictional, and bearing responses shown in Fig. 1. The nonlinear interaction between the soil and structure consisted of elastic, plastic, and gap components in series (Boulanger et al. 1999). The nonlinear backbone curves and corresponding ultimate resistances for sand and clay implemented in this study are based on the literature, as given in Table 1.

Effect of Stress History

The deposition of soils can be considered as a loading process, whereas the removal of soil due to scour can be considered as an unloading process. As a result, the remaining soil experiences a new stress state, quantified by the increase of the overconsolidation ratio (OCR) or ratio between the previous maximum stress and present stress. Lin et al. (2010, 2014b) have investigated the effect of soil stress history on the soil properties of cohesionless soils and cohesive soils. For cohesionless soils (i.e., sand), soil parameters such as friction angle, effective unit weight, and modulus of subgrade reaction can be modified due to the change of stress state after scour events. For cohesive soils (i.e., soft clay), undrained shear strain and effective unit weight are influenced by the effect of stress history before and after scour events through the OCR and scour depth. Further details on soil property changes due to stress history effects in cohesionless and cohesive materials are shown in Appendix I. Those studies focused on the influence of stress history on a single pile in the lateral direction, and the influence in the axial direction was neglected.

In comparison, Zhang and Tien (2020) have investigated the influence of stress history of layered soils on single piles in the axial direction through accounting for the change of parameters of unit shaft and bearing resistance due to the change of stress state after scour events. Both lateral and axial effects were considered in their study.

Effect of Scour Hole Dimensions

One of the common practices in modeling scour is to neglect the effect of the shape and geometry of a scour hole. However, the scour hole dimensions influence the behavior of piles in both the lateral and vertical directions. Lin et al. (2014a, 2016) have investigated the effect of scour hole dimensions on lateral behavior of a single pile for cohesionless and cohesive materials using an equivalent wedge failure model shown in Fig. 2(b). This simplified

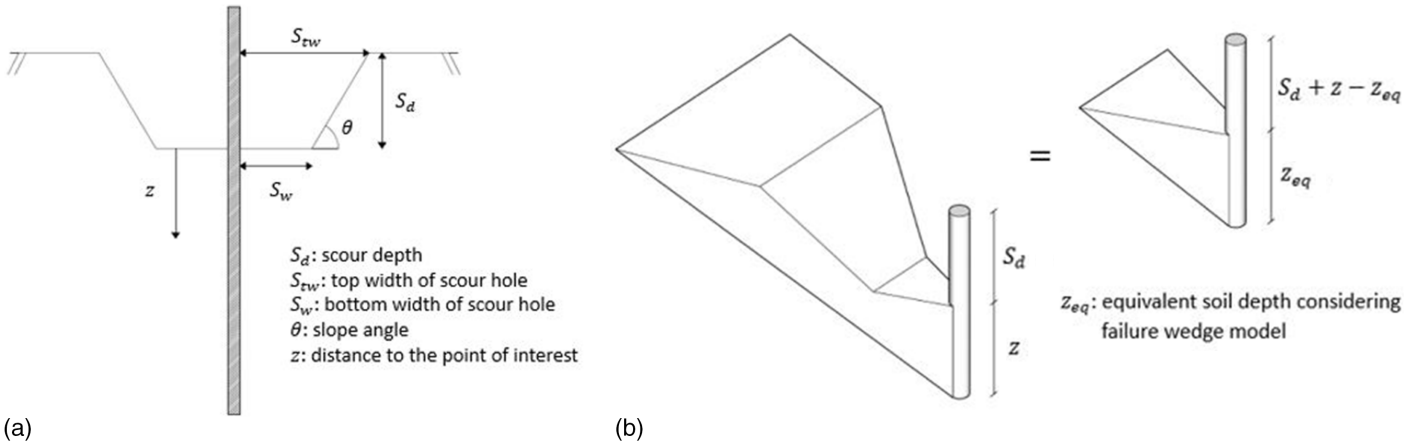

Fig. 2. (a) Geometry of scour hole; and (b) wedge failure model considering scour hole dimensions and equivalent wedge model without considering scour hole dimensions.

method accounted for the change of lateral soil resistance by considering the weight of the soil wedge above the failure plane and its interactions with the structure and soil. On the other hand, for the effect of scour hole dimensions on the axial response of the pile, Lin (2017) has proposed a closed-form solution for the additional vertical stress due to scour hole geometry by integrating Boussinesq's analytical solution. This analytical approach was applied to sands but not to clays because the undrained shear strength of clay is irrelevant to the stress change in the short term. Further details on the effect of scour hole dimensions in cohesionless and cohesive materials are given in Appendix I.

In this study, the effect of scour hole dimensions on the axial response with clayey soil was considered by modifying a dimensionless factor (α), which is a function of effective overburden pressure and directly relates to the skin friction capacity of cohesive soils. This approach is described further in the "Proposed Methodology" section. The parameters defining the scour hole dimensions are shown in Fig. 2(a) with scour depth, scour width, and slope angle. For a typical bridge, scour level (S_d) can range from 0.5 to 15 m, but most observed scour depths (i.e., up to 41%) range from 0.5 to 5.0 m (Lin et al. 2014c); scour width (S_{tw}) has been approximated as twice the scour depth (Richardson and Davis 2001); the value of slope angle (θ) depends on the bed material and is approximately equal to the angle of repose of the surrounding soils (Richardson and Davis 2001).

Zhang et al. (2016) have proposed a methodology to compute lateral resistance of soil numerically considering both scour hole geometry and possible changes of stress due to scour in soft clay with the aid of integration of Mindlin's elastic solutions. However, this methodology only applies to cohesive material, and their study did not investigate how scour hole geometry and stress history impact the vertical resistance of the soil.

Proposed Methodology

This paper proposes a generalized approach to account for the effects of soil stress history and scour hole geometry for both cohesive and cohesionless soils. In addition, the framework considers impacts on soil resistance in both lateral and vertical directions. In the proposed model, for given soil properties and scour hole geometry, the effect of scour hole geometry is first captured through computing an equivalent depth based on an equivalent wedge model at a point of interest. Next, the mechanical properties at the modified point of interest (i.e., equivalent depth from the failure-wedge model) after scour events are updated as it undergoes a new stress state, and the combined effect is accounted for through integrating these two modifications. With the equivalent depth and updated soil property values, the key parameter (i.e., P_{ult} indicating ultimate lateral resistance) for the p-y curve is obtained. Simultaneously, the total vertical effective stress, which includes soils above as well as the additional stress induced by the overburden pressure due to scour hole geometry, is computed by integrating Boussinesq's point load solution and the modified OCR (prescour stress/postscour stress) value into the framework for accounting for stress history effects, as shown in Appendix I. Postscour stress includes the contribution from the scour hole geometry through considering Boussinesq's solution.

With the values of total vertical effective stress and soil properties at the point of interest, the soil ultimate unit shaft resistance (T_{ult}) and ultimate end bearing resistance (Q_{ult}) were obtained for the t-z and q-z backbone curves. Fig. 3 presents a flowchart that summarizes the steps to obtain the key soil ultimate resistances (i.e., P_{ult}, Q_{ult}, and T_{ult}) in modeling the soil–structure interaction under scour. The process shown in Fig. 3 applies to both cohesive and cohesionless materials with corresponding nonlinear backbone relationships.

Specifics for calculating the soil resistance parameters now follow. For cohesionless soils (e.g., sand), calculating ultimate soil lateral resistance (P_{ult}) begins with considering a wedge-type failure near the surface (P_{st}) and plane-strain failure well below the ground surface (P_{sd}) as shown in Eqs. (1a) and (1b) (Reese et al. 1974). In all equations that follow, the variables with subscripts sh and shd indicate that they are affected by the effect of the soil stress history and scour hole dimensions, respectively

$$P_{st} = \gamma'_{sh} z_{shd} \left\{ \frac{K_{o(sh)} z_{shd} \tan(\phi'_{sh}) \sin(\beta)}{\tan(\beta - \phi'_{sh}) \cos(\alpha)} + \frac{\tan(\beta)}{\tan(\beta - \phi'_{sh})} [B + z_{shd} \tan(\beta) \tan(\alpha)] + K_{o(sh)} z_{shd} \tan(\beta) [\tan(\phi'_{sh}) \sin(\beta) - \tan(\alpha)] - K_a D \right\} \quad (1a)$$

$$P_{sd} = K_a B \gamma'_{sh} z_{shd} [\tan^8(\beta) - 1] + K_{o(sh)} B \gamma'_{sh} z_{shd} \tan(\phi'_{sh}) \tan^4(\beta) \quad (1b)$$

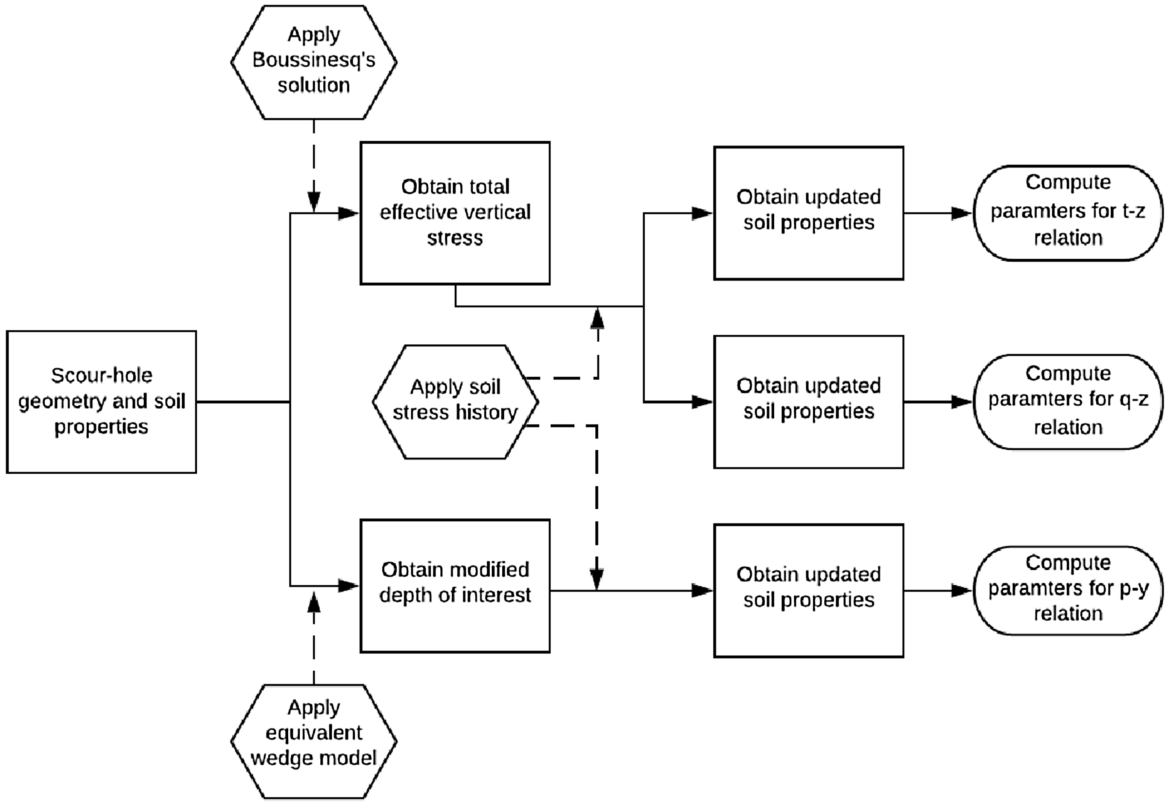

Fig. 3. Flowchart of the proposed procedure to compute parameters of soil resistance.

where z_{shd} = distance between the ground surface and point of interest, and it is an equivalent depth determined based on the failure-wedge model; γ'_{sh} = effective unit weight; β = passive failure angle; α = angle defining the shape of the failure wedge; K_a =minimum coefficient of active earth pressure; D = diameter of the pile; and ϕ'_{sh} = friction angle. There are two ways of computing the equivalent depth due to the effect of scour hole dimensions for the lateral response. The first approach is to compute the equivalent depth based on the failure-wedge model adopted in the current framework. The second approach uses Boussinesq's solution, as shown in Eq. (3), to compute the total effective vertical stress, which is then used to calculate the equivalent depth by dividing the effective unit weight. The first method is preferable in this case in terms of capturing the failure mechanism (i.e., wedge-type failure). The second method generally yields more conservative results, but it can be applied to analyze pile groups under scour conditions. Therefore, the first method was adopted in the current framework.

Ultimate skin friction resistance (T_{ult}) is a function of effective vertical stress [$\sigma'_{va(sh\&shd)}$] as shown in Eq. (2) (Touma and Reese 1974)

$$T_{\text{ult}} = 0.7\tan(\phi'_{sh\&shd})\sigma'_{va(sh\&shd)} \tag{2}$$

where $\sigma'_{va(sh\&shd)}$ is computed as in Eq. (3) (Lin 2017), where $\sigma'_{va(sh\&shd)}$ encompasses two individual portions, $\sigma'_{v(sh\&shd)}$ and $\Delta\sigma'_{v(shd)}$, which are effective vertical stress after scour considering stress history and local scour effects, and additional effective vertical stress due to scour hole dimensions, respectively

$$\sigma'_{va(sh\&shd)} = \sigma'_{v(sh\&shd)} + \Delta\sigma'_{v(shd)} \tag{3a}$$

$$\sigma'_{v(sh\&shd)} = z\gamma'_{sh\&shd} \tag{3b}$$

$$\Delta\sigma'_{v(shd)} = z\gamma'\tan(\theta)\left[\frac{\frac{S_d}{\tan(\theta)} + S_{bw}}{\sqrt{\left(\frac{S_d}{\tan(\theta)} + S_{bw}\right)^2 + z^2}} - \frac{S_{bw}}{\sqrt{S_{bw}^2 + z^2}}\right] \tag{3c}$$

The parameters S_d, S_{bw}, and θ are as defined in Fig. 2. Both soil stress history and local scour conditions affect the friction angle ($\phi'_{sh\&shd}$) as well as effective vertical stress after scour [$\sigma'_{v(sh\&shd)}$], as indicated in Eqs. (2) and (3*b*). For the lateral response, the friction angle, as presented in Eq. (1), was only a function of the stress history because the local scour effect was accounted for through the calculated equivalent depth from the equivalent wedge model. The impact of scour hole dimensions was also manifested through the inclusion of the additional effective vertical stress [$\Delta\sigma'_{v(shd)}$] due to scour, as shown in Eq. (3*c*). Eq. (4) presents an equation for computing the ultimate end bearing resistance (Mayerhof 1976)

$$Q_{\text{ult}} = N_{q(sh\&shd)}\sigma'_{vbot(sh\&shd)} \tag{4}$$

where $N_{q(sh\&shd)}$ = bearing capacity factor, which is a function of $\phi'_{sh\&shd}$, where the actual value of the capacity factor is dependent on the friction angle and installation method; this study adopted Meyerhof values of N_q for piles; and $\sigma'_{vbot(sh\&shd)}$ = effective vertical stress at the bottom of the pile, which can be expressed as a function of $\gamma'_{sh\&shd}$, and it is affected by both stress history and scour hole dimension effects.

Previously, Lin and Jiang (2019) have investigated pile tension capacity in sands. That study considered the impact of scour hole geometries only, whereas the present study focused on the axial force-displacement response from the combined effects of scour

hole geometries and soil stress history. Eq. (5) presents the expression for the modified tension capacity that combines the effects of stress history and scour hole dimensions based on the proposed framework

$$R_s = \int_0^L \pi D K \sigma'_{va(sh\&shd)} \tan(\delta_{sh\&shd}) dz \quad (5)$$

where K = coefficient of lateral earth pressure, which is taken as 0.9 for the calculation of tension capacity; $\delta_{sh\&shd}$ = friction angle of the soil–pile interface, and it is chosen as the soil friction angle in this study; and $\sigma'_{va(sh\&shd)}$ = vertical effective stress of the soil at the pile after scour, and it is defined in Eq. (3). Comparison of results from this study with those from Lin and Jiang (2019) is provided in the section "Axially Loaded Piles in Sand."

Calculating the soil resistance for cohesive soils (e.g., clay) followed a similar approach as for sand but with different nonlinear backbone curves and corresponding equations for the ultimate resistance parameters. The procedure started with determining the equivalent depth (z_{shd}) based on the failure-wedge model, which accounts for the effect of scour hole geometry. Ultimate lateral resistance was then computed based on the smaller of the two values shown in Eq. (6) (Matlock 1970)

$$P_{\text{ult}} = \min\left\{\left(3 + \frac{\gamma'_{sh}}{C_{u(sh)}} z_{shd} + \frac{J}{B} z_{shd}\right) C_{u(sh)} B, 9 C_{u(sh)} D\right\} \quad (6)$$

where $C_{u(sh)}$ = undrained shear strength of soft clay; and J = constant with the value set to be 0.5. The ultimate skin friction resistance of clay was determined according to Eq. (7) (Tomlinson and Boorman 2001)

$$T_{\text{ult}} = \alpha_{sh\&shd} C_{u(sh\&shd)} \quad (7)$$

where $\alpha_{sh\&shd}$ = dimensionless factor with the constraint of being not greater than 1; and $C_{u(sh\&shd)}$ = undrained shear strength of clay, which is different from the one in Eq. (6) for the lateral response. Both of these parameters are affected by soil stress history and scour hole geometry through parameter ψ based on API (2000) as shown in Eqs. (8*a*) and (8*b*)

$$\alpha_{sh\&shd} = 0.5\psi^{-0.5}, \quad \psi \le 1 \quad (8a)$$

$$\alpha_{sh\&shd} = 0.5\psi^{-0.25}, \quad \psi > 1 \quad (8b)$$

where

$$\psi = \frac{C_{u(sh\&shd)}}{\sigma'_{va(shd\&shd)}} \quad (8c)$$

Thus, the skin friction resistance of clay (T_{ult}) was influenced by both soil stress history and scour hole dimensions. Finally, the end-bearing resistance (Q_{ult}) of clay was based on Terzaghi's bearing capacity theory (Terzaghi 1943), with the relation simplified to Eq. (8) due to the characteristics of cohesive soils and piles

$$Q_{\text{ult}} = 9 A_p C_{u(sh\&shd)} \quad (9)$$

where A_p = cross-sectional area of the pile.

The expression for the tension capacity in clay can be modified based on the proposed framework as shown in Eq. (10)

$$R_s = \int_0^L \pi D \alpha_{sh\&shd} C_{u(sh\&shd)} dz \quad (10)$$

Eq. (10) accounts for both stress history and scour hole dimension effects by incorporating the modified values of undrained shear strength ($C_{u(sh\&shd)}$) and the dimensionless factor ($\alpha_{sh\&shd}$), as shown in Eqs. (7) and (8). The implementation of Eq. (10) is presented in the section "Axially Loaded Piles in Clay."

Tables 2–4 summarize the methodologies to compute ultimate resistance for cohesionless and cohesive soils for P_{ult}, T_{ult}, and Q_{ult}, respectively. The novelty of the proposed approach is to combine all soil effects in the updating of soil parameters due to scour for both cohesive and cohesionless soils and in both lateral and vertical directions. Results provided in subsequent sections show the importance of including these combined effects of soil stress history and scour hole dimensions in the assessment of scoured bridges. The proposed framework not only presents a comprehensive evaluation of the pile's lateral and axial responses considering the combined soil effects under scour phenomenon, but it also provides a

Table 2. Methodologies to obtain P_{ult}

P_{ult}	Sand	Clay
Soil stress history	OCR approach [Eq. (1) and Appendix I (Fig. 21)]	OCR approach [Eq. (6) and Appendix I (Fig. 22)]
Scour hole dimensions	Equivalent depth approach with failure-wedge model [Eq. (1) and Appendix I (Fig. 23)]	Equivalent depth approach with failure-wedge model [Eq. (6) and Appendix I (Fig. 24)]

Table 3. Methodologies to obtain T_{ult}

T_{ult}	Sand	Clay
Soil stress history	OCR approach [Eq. (2) and Appendix I (Fig. 21)]	OCR approach [Eq. (7) and Appendix I (Fig. 22)]
Scour hole dimensions	OCR approach with Boussinesq's solution [Eqs. (2) and (3), and Appendix I (Fig. 21)]	OCR approach with Boussinesq's solution [Eqs. (3), (7), and (8) and Appendix I (Fig. 22)]

Table 4. Methodologies to obtain Q_{ult}

Q_{ult}	Sand	Clay
Soil stress history	OCR approach [Eq. (4) and Appendix I (Fig. 21)]	OCR approach [Eq. (9) and Appendix I (Fig. 22)]
Scour hole dimensions	OCR approach with Boussinesq's solution [Eqs. (4) and (3) and Appendix I (Fig. 21)]	OCR approach with Boussinesq's solution [Eqs. (3) and (9) and Appendix I (Fig. 22)]

Table 5. Summary of experimental and numerical data used in validation and verification of the proposed framework

Analysis type	Soil type	References	
		Field testswithout scour	Numerical modelswith scour
Laterally loaded piles	Sand	Cox et al. (1974)	Lin et al. (2010, 2014a)
	Clay	Reese and Van Impe (2001)	Lin et al. (2014b, 2016) and Zhang et al. (2016)
Axially loaded piles	Sand	Briaud et al. (1989)	—
	Clay	O'Neill et al. (1982)	—

tool that facilities future pile design as well as a platform for future research. The following section presents comparisons between the proposed model and other soil models and experimental tests for verification and validation in terms of multiple response parameters for a selected single-pile structure.

Analyses of the Proposed Methodology

The proposed framework was implemented in the open-source finite-element platform OpenSees version 3.3.0 (McKenna 1997), with the soil–structure interaction modeled as shown in Fig. 1. The validation and verification focused on the response of laterally and axially loaded piles in sand and clay. Table 5 gives the details in terms of analysis type, soil type, field tests, and numerical models found from the existing literature. The numerical result from the proposed model was first validated with experimental field test data for both lateral and axial responses without considering scour events. This validation acted as a benchmark to ensure the proposed model yielded reliable results before considering the scour phenomenon.

Next, after an extensive literature review, because experimental tests of laterally and axially loaded piles in the presence of scour are scarce, the authors used existing numerical results to verify the proposed framework considering scour. The numerical models for sand were selected from Lin et al. (2010, 2014a), which account for the effects of stress history and scour hole dimensions, respectively, in the presence of scour. Lin et al. (2014b, 2016) focused on effects of stress history and scour hole dimensions, respectively, for a laterally loaded pile in clay. The numerical response considering the combined effect of stress history and scour hole dimensions from Zhang et al. (2016) were also compared with the proposed model for verification. Numerical results for axially loaded piles considering scour do not exist in the literature and were unavailable for comparison, as indicated with a dash in Table 5.

Table 6. Sand properties for Mustang Island

Property	Value
Critical friction angle (degrees)	28.5
Effective unit weight (kN/m^3)	10.4
Relative density (%)	70 (depth < 3 m) and 90 (depth ≥ 3 m)
Maximum void ratio	1.0
Minimum void ratio	0.598
Specific gravity	2.65

Laterally Loaded Piles in Sand

The laterally loaded pile field test in sand was performed in a modified soil profile from Mustang Island, Texas (Cox et al. 1974), reported to be uniform-graded fine sand. The properties of the sand are listed in Table 6. The geometries of the pile and the applied load (P_h) are shown in Fig. 4(a). The moment of inertia and elastic modulus of the pile were 8.1×10^{-4} m^4 and 2.0×10^8 kN/m^2, respectively. Fig. 4(b) shows the ground line deflection versus laterally applied load at the pile head without considering scour.

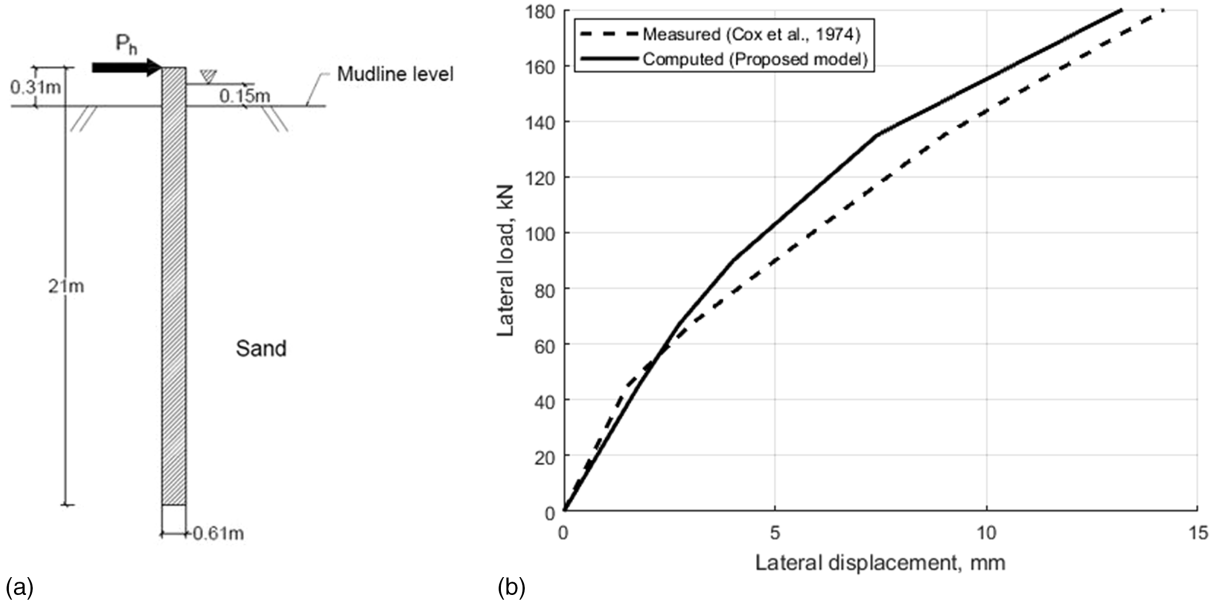

Fig. 4. (a) Laterally loaded pile in sand; and (b) deflection at the ground line versus laterally applied load for measured data compared with proposed model result without considering scour.

J. Geotech. Geoenviron. Eng., 2022, 148(5): 04022028

The displacement curves for the measured data and values obtained from the proposed model tracked closely, with a maximum displacement difference of 1.58mm. The difference can be attributed to the estimation of the soil resistances and empirical equations used in the numerical modeling such as the p-y relation.

For scour scenarios, due to the scarcity of existing experimental data, the authors chose to verify the proposed model with results from existing numerical models. Fig. 5 presents a comparison of the proposed approach with the results from Lin et al. (2010) for 3-m scour depth (S_d) and 39° slope angle (θ). As opposed to Lin et al.'s (2010) model, which only considered the effect of stress history in sand, the proposed model is capable of capturing the impact from scour hole dimensions. The results for the proposed model shown in Fig. 5 consist of three different values of bottom scour width (S_w): 0, D, and ∞, where D is the diameter of the pile with a value of 0.61 m. Scour width of ∞ is equivalent to neglecting scour hole dimensions. From Fig. 5, as the scour width increased, the magnitude of the lateral deflection also increased as the impact from the scour hole dimensions decreased. The case of bottom scour width equal to ∞ for the proposed model was closest to the Lin et al. (2010), which neglected the effect of scour hole dimensions and only accounted for the effect of stress history in sand. The discrepancy between Lin et al.'s (2010) model and the proposed model with the infinite value of scour width was mainly due to the use of different p-y relations in the lateral soil spring.

For comparison, Fig. 6 provides the results from Lin et al. (2014a), which only considered the effect of scour hole dimensions, with those from the proposed model for a scour depth of $3 \times D$, bottom scour width of 0, and slope angle of 39°. The proposed approach included both scour hole dimension and soil stress history effects. The stress history effect slightly reduced the effective unit weight, relative density, and modulus of subgrade reaction of the remaining sand. However, the unloading process with scour increased the friction angle and overconsolidation ratio, which had a greater impact on the lateral resistance of sand, resulting in increased soil lateral resistance. Therefore, a reduced lateral deflection was expected with the inclusion of stress history effects. The results in Fig. 6 show this with the proposed model yielding smaller lateral deflections at the ground level due to its ability to include the effect of stress history.

To investigate the impact of including soil effects in the analysis of laterally loaded piles in sand, Fig. 7 shows a comparison of estimated pile deflection versus laterally applied load both with and without considering the combined soil effect under varying scour conditions. The combined soil effect is indicated with an abbreviation of s.e. Several observations can be made based on the results shown in Fig. 7. First, an increase in scour depth increased the flexibility of the pile in sand with a larger scour depth, leading to larger values of pile lateral deflection. Second, the combined soil effect increased the lateral soil resistance, reducing the deflection in comparison with not considering soil effects for a given value of applied load and scour depth. Third, the impact of the combined soil effect increased as scour depth increased, as observed by the increasing

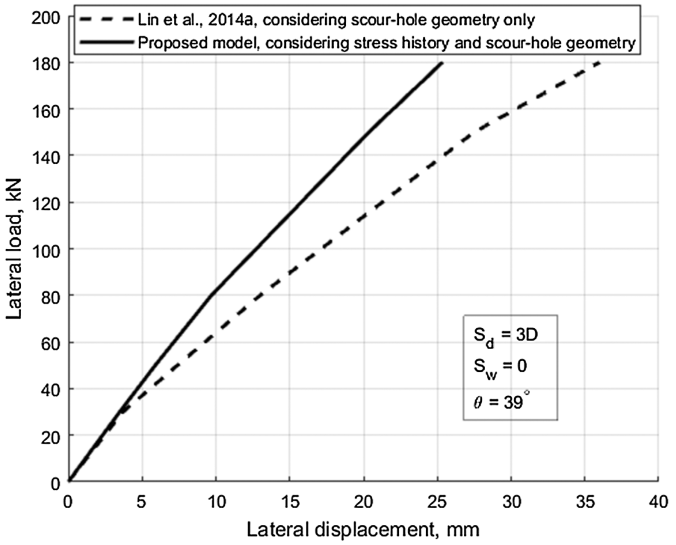

Fig. 6. Comparison between numerical models of deflection at the ground line versus laterally applied load with scour depth of $3 \times D$, scour width of 0, and slope angle of 39° in sand.

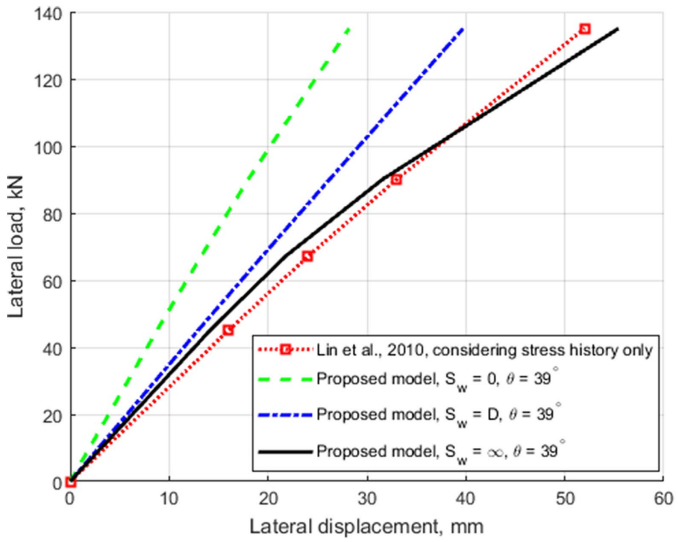

Fig. 5. Comparison between numerical models of deflection at the ground line versus laterally applied load with scour depth of 3 m in sand.

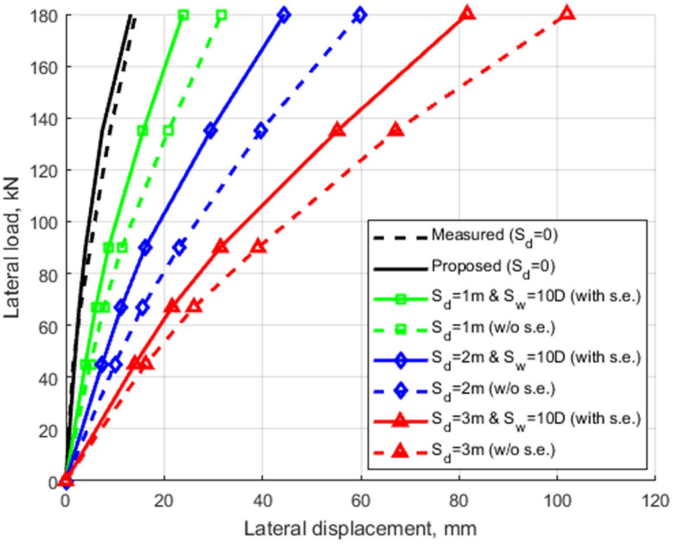

Fig. 7. Comparison of deflection at the ground line versus laterally applied load with and without considering combined soil effect under varying scour conditions in sand.

difference between the solid line and dashed line as scour depth increased. In summary, not considering soil effects could lead to an overly conservative design in terms of the lateral response of a pile in sand.

Table 7. Properties of soft clay near Lake Austin, Texas

Property	Value
Effective unit weight (kN/m^3)	10
Water content (%)	44.5
Compression index	0.38
Swelling index	0.076
Strain at half of maximum stress	0.012
Effective friction angle (degrees)	20

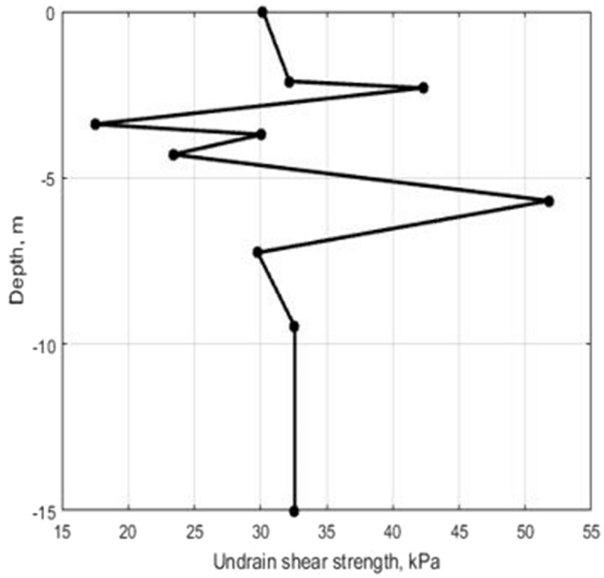

Fig. 8. Distribution of undrained shear strength of soft clay. (Data from Reese and Van Impe 2001.)

Laterally Loaded Piles in Clay

The field tests for laterally loaded piles in clay are in a soft clay profile near Austin, Texas. The soil properties are summarized in Table 7 and categorized as fat clay based on the Unified Soil Classification System. The swelling index was estimated empirically as 1/5 of the compression index (Kulhawy and Mayne 1990). The distribution of undrained shear strength was measured by Reese and Van Impe (2001) with values plotted in Fig. 8. The parameters of the pile were obtained from Reese and Van Impe (2001) with a length of 12.8 m, an outer diameter of 0.319 m, a thickness of 0.0127 m, a moment of inertia of 1.44×10^{-4} m^4, and elastic modulus of 218 GPa. Fig. 9(a) shows the geometry of the pile, and Fig. 9(b) gives a comparison between the proposed model result and experimental data in terms of pile head deflection versus laterally applied load without considering scour. The two results followed a close trend, with an average percentage difference of 14%. Although no scour was considered in the experimental test, the comparison provided a benchmark for further study of the proposed model under scour conditions.

Fig. 10 presents a comparison of the pile head deflection versus laterally applied load between Lin et al.'s (2014b) model and results from the proposed model with scour depth of $10 \times D$, where D is 0.319 m, which is also the diameter of the pile. Results for the proposed model for a slope angle of 40° and bottom scour width of 0, $5 \times D$, and ∞ are shown. The scour width of ∞ indicates the impact of scour hole dimensions was neglected. As a result, the result from Lin et al. (2014b) that captures only the effect of stress history yielded the same result as the proposed model for scour width of ∞. Both the proposed model and Lin et al. (2014b) adopted the same p-y curve (Matlock 1970). In comparison, for the other curves, the proposed model considered both the effects of stress history and scour hole dimensions. From Fig. 10, the effect of scour hole dimensions increased the lateral resistance of clay, leading to an increase in pile head deflection as the bottom scour width increases from 0 to ∞.

Fig. 11 presents a comparison of deflection between three different numerical models under scour depth of $6 \times D$, scour width of 0 m, and slope angle of 40°. The numerical result from

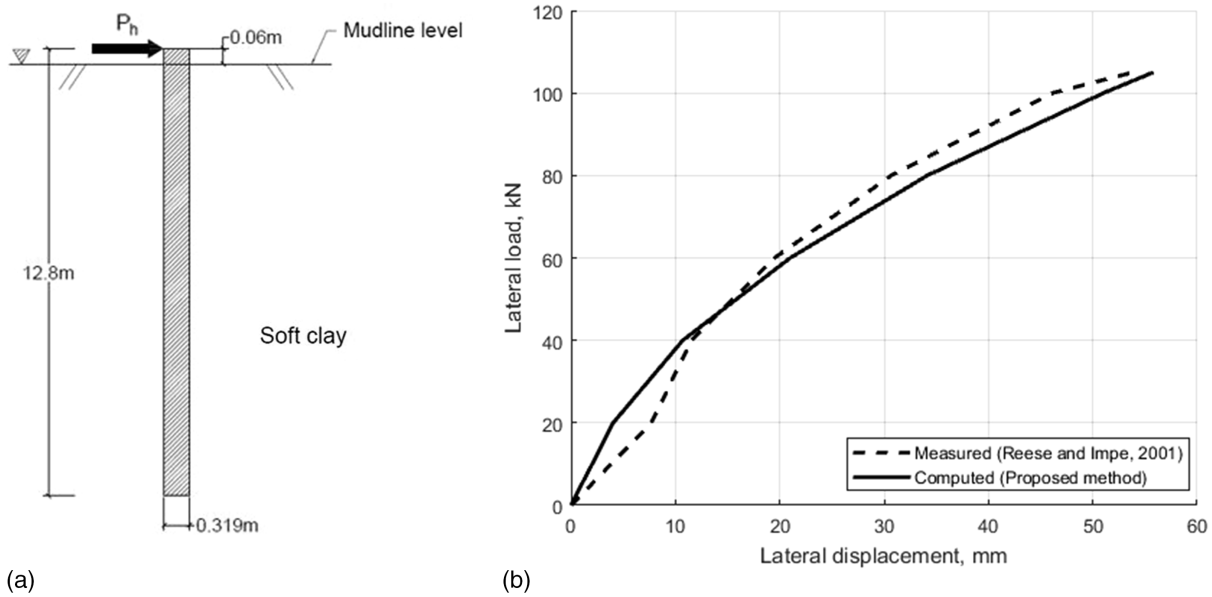

Fig. 9. (a) Laterally loaded pile in soft clay; and (b) deflection at the pile head versus laterally applied load for measured data compared with proposed model result without considering scour.

J. Geotech. Geoenviron. Eng., 2022, 148(5): 04022028

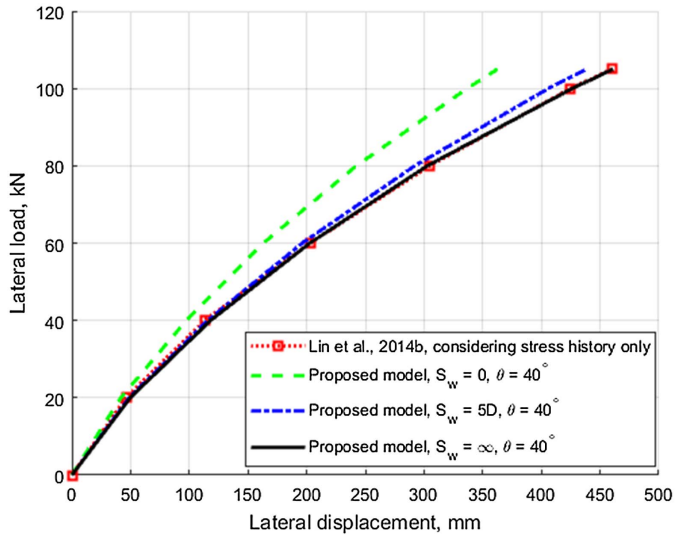

Fig. 10. Comparison between numerical models of pile head deflection versus laterally applied load with scour depth of $10 \times D$ in soft clay.

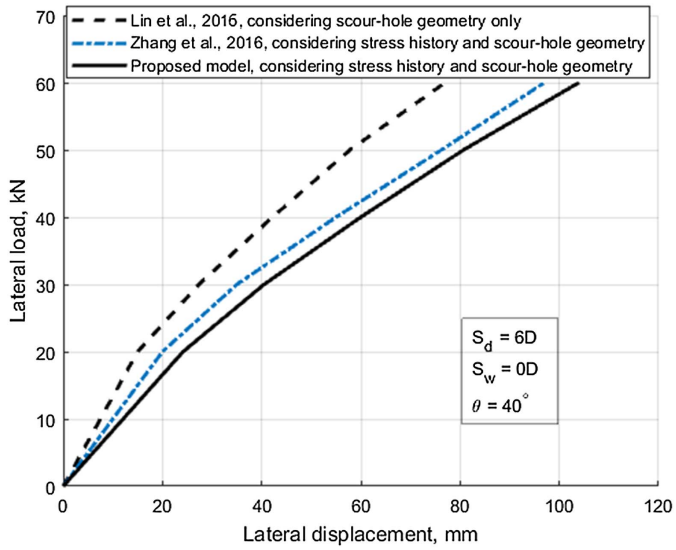

Fig. 11. Comparison between numerical models of deflection at the pile head versus laterally applied load with scour depth of $6 \times D$, scour width of 0, and slope angle of 40° in soft clay.

Liang et al. (2015) captured only the impact of scour hole dimensions. In comparison, both numerical results from Zhang et al. (2016) and the proposed model were able to account for the combined effect of stress history and scour hole dimensions in clay. As shown in Fig. 11, the soil stress history reduced the lateral resistance of clay, increasing the pile head deflection. The Zhang et al. (2016) and proposed models tracked closely with the proposed model, yielding a slightly more conservative result. The increase in pile head displacement estimated in clay when the combined stress history and scour hole dimensions effects were considered differed from the effect observed in sand.

Fig. 12 investigates the soil effect as a function of scour depth, showing the estimated deflection versus laterally applied load with and without considering the combined soil effect under varying

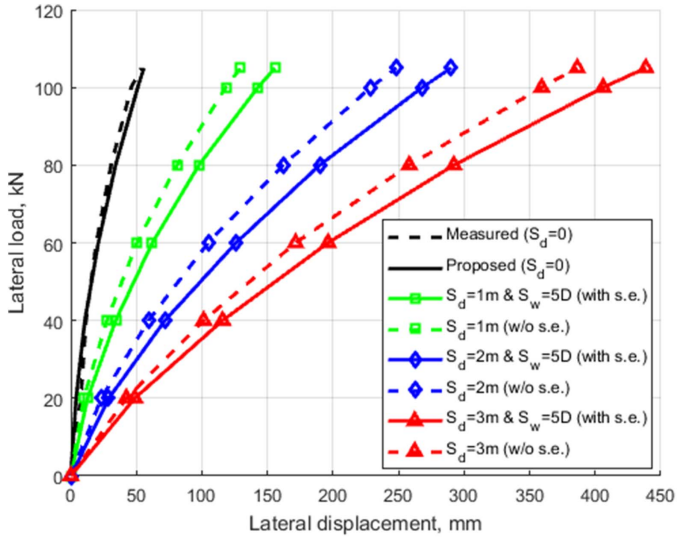

Fig. 12. Comparison of deflection at the pile head versus laterally applied load with and without considering combined soil effect under varying scour conditions in soft clay.

scour conditions in soft clay. The observations made from Fig. 12 are as follows. First, as scour depth increased, the lateral load resistance of the clay decreased, leading to larger deflection values. Second, accounting for the combined soil effect led to increased estimated pile head deflections. However, unlike the results shown in Fig. 7 for sand, the combined soil effect in clay did not appear to be amplified as scour depth increases. This is because unlike in sand, there are counteracting effects in clay. The influence of stress history in clay was counteracted by the influence of scour hole dimensions as scour depth increased. Third, because including soil effects led to larger estimated deflections, the impact of stress history was the dominating factor in clay in comparison with the impact of scour hole dimensions across varying scour depths. This phenomenon was observed from the differences in estimated pile head deflection values between the dashed and solid lines in Fig. 12.

Axially Loaded Piles in Sand

This section examines the pile axial behavior. The goal is to illustrate that the proposed method is capable of predicting the settlement of axially loaded piles under scour conditions considering the combined soil effect. The field test of axially loaded piles in sand was reported by Briaud et al. (1989). The soil was made of a hydraulic fill with clean sand with a shear modulus of 38.3 MPa, friction angle of 35°, and dry unit weight of 15.7 kN/m^3. As shown in Fig. 13(a), the closed-end steel pile with a diameter of 273 mm and a wall thickness of 9.3 mm was driven to a depth of 9.15 m below the mudline in the sand. The steel pile had a Young's modulus of 2.1×10^5 MPa.

From Castelli and Maugeri (2002), a linearly increasing unit skin shaft capacity ranging from zero at the mudline level up to 45 kPa at the pile base should be used for the numerical model. The analysis of the axially loaded pile was performed in OpenSees, with the load-settlement response plotted in Fig. 13(b). The measured experimental data along with computed numerical data from Castelli and Maugeri (2002) and the proposed model without considering scour are shown. The proposed model tracked both the experimental and previous numerical results closely, with an average percentage difference of 17.2% and 11.6% compared with the

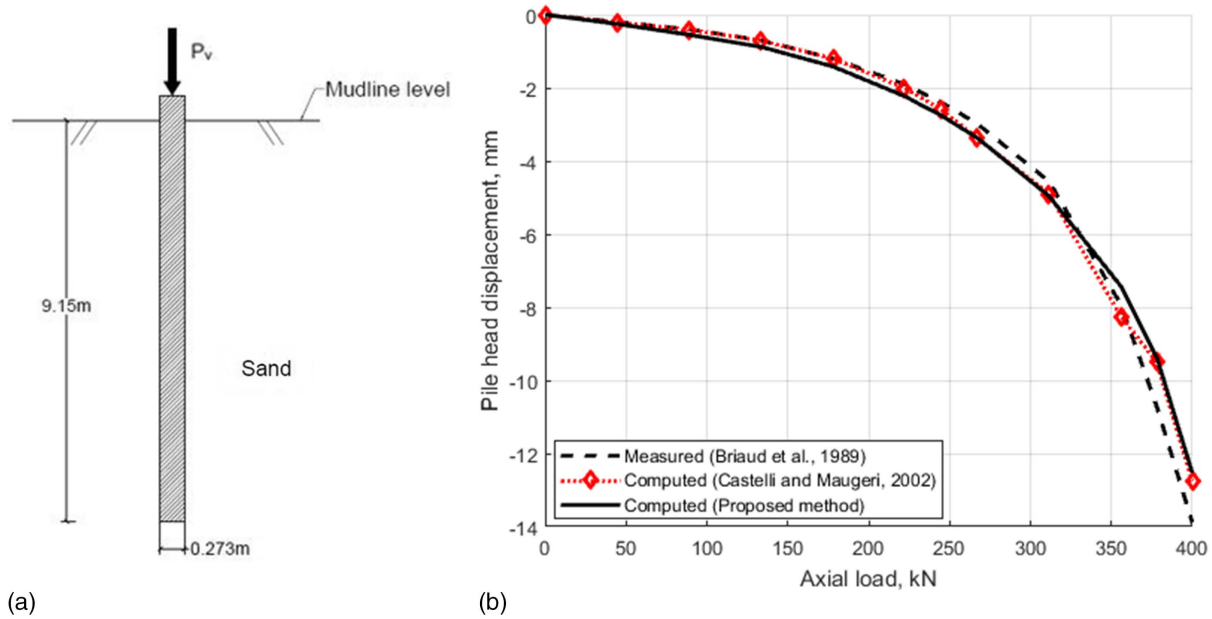

Fig. 13. (a) Axially loaded pile in sand; and (b) settlement at the pile head versus axially applied load for measured data compared with proposed model result without considering scour.

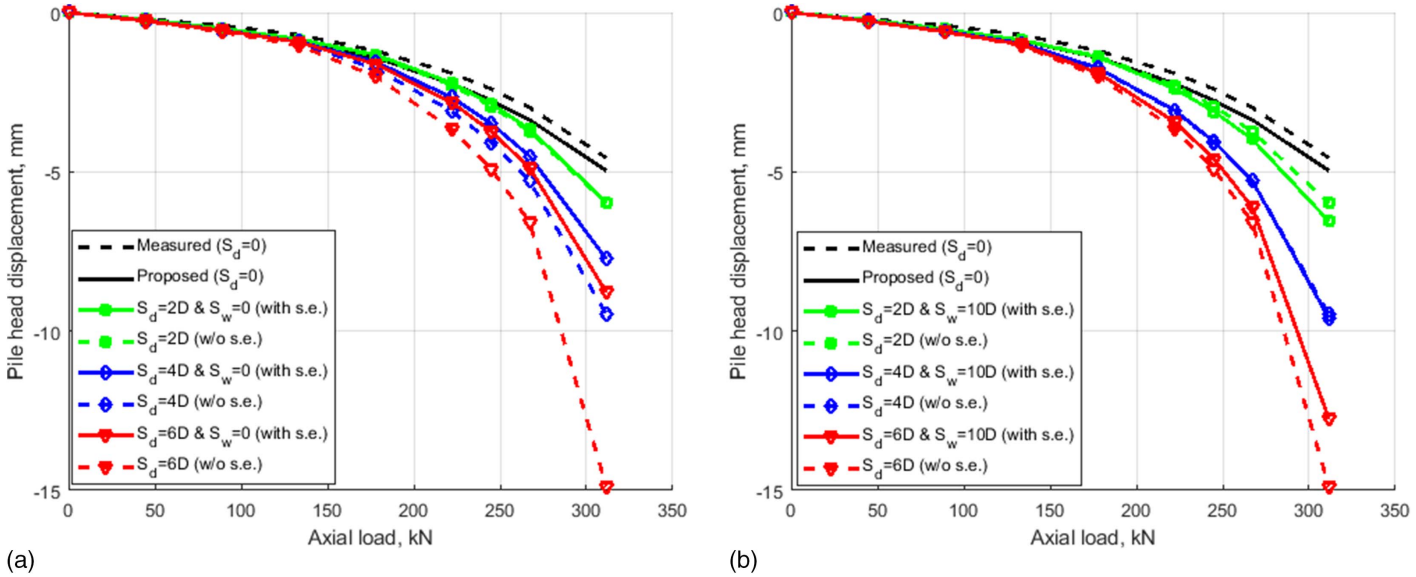

Fig. 14. Load-settlement curves at the pile head with varying scour depths and the values of (a) 0; and (b) $10 \times D$ for bottom scour width in sand.

experimental data and numerical data from Castelli and Maugeri (2002), respectively. The validation shown in Fig. 13(b) serves as a benchmark for further study of the pile response under scour conditions.

Before computing the response of the axially loaded pile under scour conditions with the proposed method, several assumptions need to be addressed. The slope angle and relative density were taken as 30° and 55%, respectively, for medium dense sand, and the critical friction angle was taken to be 28.5°. The effective unit weight of sand was back-calculated based on the value of the dry unit weight of 15.7 kN/m^3 and assumed a specific gravity of 2.65, which gives a value of 9.78 kN/m^3. Fig. 14 gives the load-settlement curves for varying scour depths and two different values of bottom scour width with and without considering the combined soil effect. Scour depths varied from $2 \times D$ to $6 \times D$ with the value of D equal to 0.273 m.

Figs. 14(a and b) give results for a bottom scour width of 0 and $10 \times D$, respectively. From Fig. 14, as scour depth increased, the ability of the soil to resist a vertical load decreased, leading to increased pile head settlements. Comparing Figs. 14(a and b), the scour width had a significant impact on the vertical behavior of the pile. As the bottom scour width increased, considering the combined soil effect led to a significant increase in the settlement expected under an axial load. This is because by increasing the scour width, the vertical load-carrying capacity was reduced in the sand because the scour hole geometry provided additional vertical stress as shown in Eq. (3), which in turn decreased the vertical resistance in the sand.

Fig. 15 further investigates the impact of scour width, showing load-settlement curves for scour depths of $2 \times D$ and $4 \times D$ with varying scour width ranges from 0 to ∞. Scour width values of 0 and ∞ provided an upper and lower bound, respectively, for a given scour depth, which was consistent with the previous observation regarding the role of scour hole dimensions in the lateral response shown in Fig. 10. A scour width of ∞ implies the effect of scour hole dimensions was neglected. Comparing it with the results without considering the soil effect shows that the impact of stress history weakened the vertical response of the pile in sand, differing from the lateral behavior in sand, which was more greatly affected by the friction angle. This is because the reduction of effective unit weight (Lin et al. 2010) during the stress history loading and unloading process plays an important role in determining the vertical resistance of the sand. For example, Fig. 15(b) shows that $S_d = 4 \times D$ [without (w/o) s.e.] yielded smaller values of settlement than $S_d = 4 \times D$ and $S_w = \infty$ (with s.e.). This result is due to the reduction of effective unit weight of the cohesionless soil as a result of the soil stress history. $S_d = 4 \times D$ (w/o s.e.) yielded similar values of settlement with $S_d = 4 \times D$ and $S_w = 10 \times D$ (with s.e.) because the effect of the reduction of effective unit weight on the vertical response due to stress release in the soil counteracted the increase of vertical resistance due to local scour.

To take a closer look at the impact of soil stress history on the values of T_{ult} and Q_{ult}, two tables providing detailed soil properties and ultimate soil resistance values are presented in Appendix II. One table presents friction angle, OCR, effective unit weight, T_{ult}, and Q_{ult} for the pile settlement response under $4 \times D$ scour depth with and without considering the stress history effect. The effect of stress history slightly increased T_{ult} due to the increase of friction angle. However, the value of Q_{ult} reduced, which led to the increase of settlement. The reduction of effective unit weight (γ'_{sh}) due to stress history was the main reason leading to the reduction of end-bearing resistance by 4.4%.

To further understand the change of effective unit weight and end-bearing resistance, the next table in Appendix II presents the soil parameters considering a higher relative density of 65% as opposed to 55% relative density in the previous table in Appendix II. As the relative density of sand increased, the reduction of effective unit weight became less significant, leading to a 2.6% drop (compared with a 4.4% drop for 55% relative density) in end-bearing resistance. The effective unit weight before considering scour was 9.78 kN/m^3.

Table 8 summarizes the impact of stress history, showing that including the effect of stress history in sand increases estimated pile settlement by up to 34.1% at $4 \times D$ scour depth and 311.5 kN axial load. Therefore, neglecting to include the impact of stress history in the analysis could lead to an unconservative design. Although in this case, the load-settlement curve not considering soil effects was close to that considering stress history and scour hole geometry with scour width of $10 \times D$, one cannot rely on these coincidental outcomes, and varying levels of scour depth, scour width, and others., would result in varying settlement curves. Therefore, it is critical to be able to quantitatively include the impacts of stress history and scour hole dimensions in the analysis of piles subject to scour as presented in this paper to accurately estimate pile behavior under varying conditions. Scour depth level impacted the reduction of effective unit weight and thus the end-bearing resistance and magnitude of pile settlement in sand, as shown in Fig. 15. The increase in the pile settlement due to the

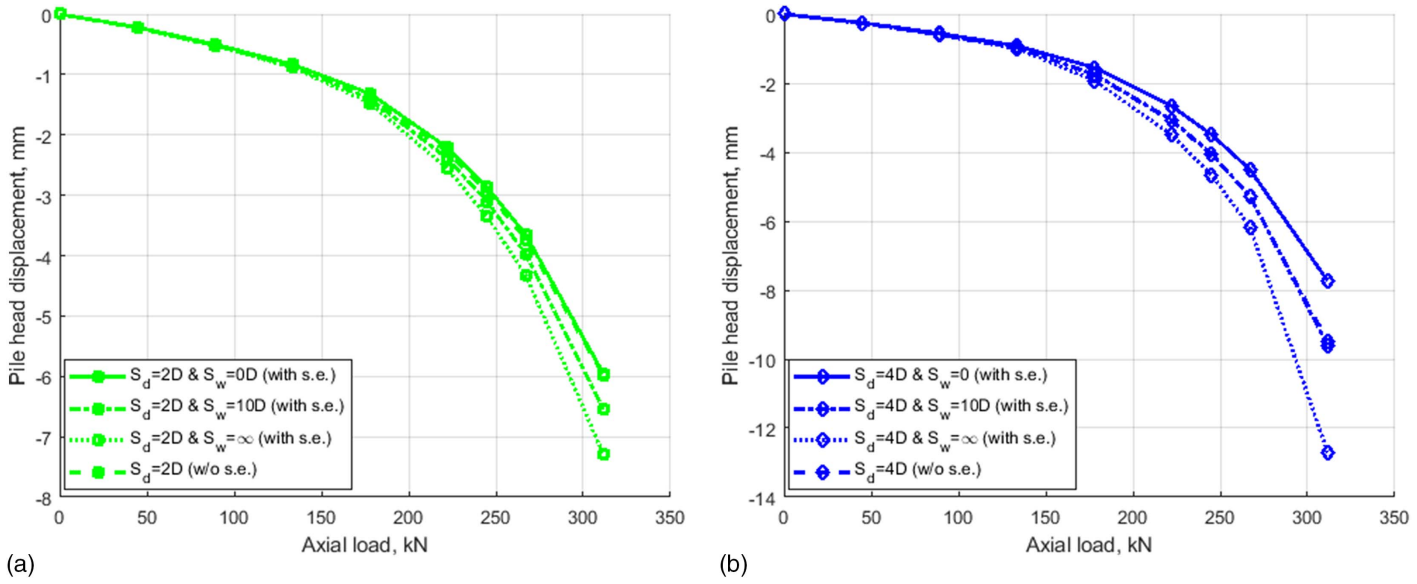

Fig. 15. Load-settlement curves at the pile head with (a) $2 \times D$; and (b) $4 \times D$ scour depths and varying bottom scour widths in sand.

Table 8. Summary of settlement values considering $4 \times D$ scour depth with and without including the effect of stress history in sand

Parameter	DP #1	DP #2	DP #3	DP #4	DP #5	DP #6	DP #7	DP #8
Axial load (kN)	44.5	89	133.5	178	222	245	267	311.5
Settlement without soil effect (mm)	0.26	0.59	0.97	1.76	3.09	4.08	5.29	9.47
Settlement with $S_w = \infty$ (mm)	0.26	0.60	1.00	1.93	3.49	4.67	6.17	12.70
Increase due to the effect of stress history (%)	0.0	1.3	2.7	9.3	12.7	14.4	16.8	34.1

Note: DP = data point.

soil stress history effect at 311.5 kN loading was 21.7% for the $2 \times D$ case and 34.1% for the $4 \times D$ case.

The tension capacity of a single pile in sand is now investigated. To assess the impact of the modified tension capacity considering both stress history and scour hole dimensions effects as shown in Eq. (5), Fig. 16 presents the tension capacity ratio ($R_{s(\text{postscour})}/R_{s(\text{prescour})}$) as a function of scour depth and scour width. Parameters of the loose sand soil profile and pile geometry are summarized in Table 9 and were taken from Lin and Jiang (2019), which considers the impact of scour hole dimensions only, to facilitate comparison of the results.

Two approaches are evaluated and compared herein. In Fig. 16, the analytical solution refers to Boussinesq's point load equation based on Lin (2017). It can account for the impact of scour hole dimensions with a closed-form expression and was also used for comparison by Lin and Jiang (2019). The proposed method includes both scour hole dimensions and soil stress history effects based on the proposed framework, as shown in Fig. 3.

As expected, the tension capacity reduced as bottom scour width increased under varying scour depths due to the impact of the scour hole geometry. Comparing the results from the proposed method with the analytical solution for the case with $S_w = 4 \times D$, the proposed method yielded relatively higher postscour tension capacities than the analytical solution due to the increased friction angle resulting from the soil stress history. When the bottom scour width was equal to $2 \times D$, $4 \times D$, and 0, the tension capacity ratio was slightly over unity for the proposed method at lower scour depths.

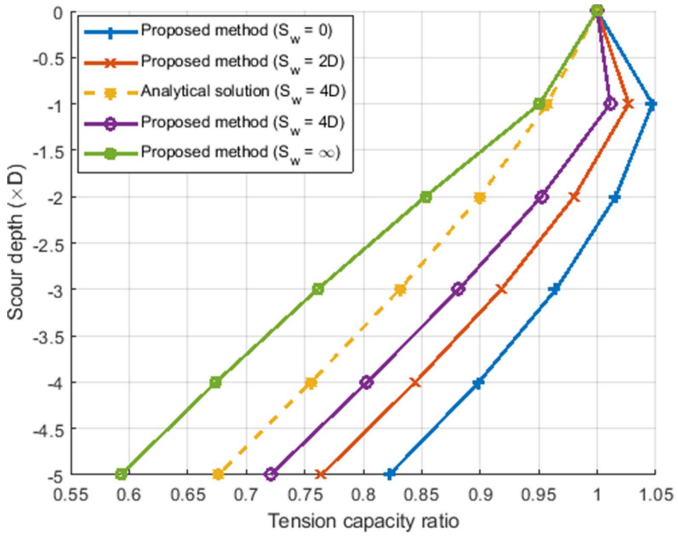

Fig. 16. Tension capacity ratios in sand with various scour depths and scour widths.

Table 9. Soil and pile parameters in loose sand

Parameter	Property	Value
Soil parameters	Saturated unit weight (kN/m^3)	19
	Effective friction angle (degrees)	28
	Void ratio	0.7
	Poisson's ratio	0.3
Pile parameters	Diameter (m)	1
	Length (m)	20
	Elastic modulus (MPa)	24,000
	Poisson's ratio	0.15

Source: Data from Lin and Jiang (2019).

This is because the reduction of tension capacity was compensated for by the soil effect at these low scour levels. Namely, the additional effective vertical stress due to scour hole dimensions and increase of soil friction angle due to scour provided extra tension capacity that helped strengthen the tensile response.

Axially Loaded Piles in Clay

The axially loaded pile tests reported by O'Neill et al. (1982) were in stiff overconsolidated clay. The closed-end steel pile with an external radius of 0.137 m and thickness of 9.3 mm was driven in stiff clay with an embedded length of 13.1 m as shown in Fig. 17(a). According to the back-analysis by Castelli and Maugeri (2002), a linearly increasing undrained shear strength profile was adopted. The value of the reduction factor (α) shown in Eq. (7) was taken as 0.40, which resulted in a unit shaft capacity that varied linearly from 19 kN/m^2 at the surface to 93 kN/m^2 at the base. The soil deformation modulus can be back-calculated with a value of 195×10^3 kPa, and the elastic modulus of the steel pile was taken as 210 GPa. Under the assumption of a constant value of α, the undrained shear strength can be back-calculated based on Eq. (7), and effective unit weight can be computed based on Eq. (8) once the value of undrained shear strength is known.

A comparison of load-settlement curves between the experimental data and numerical results from Castelli and Maugeri (2002) and the proposed model without scour is shown in Fig. 17(b). The curves tracked closely with an average percentage difference of 10% between experimental data and the proposed method. This comparison serves as a benchmark for further load-settlement analysis considering soil effects in the presence of scour events.

The following investigates the impact of including soil effects in the assessment of pile displacement under varying scour scenarios. Fig. 18 gives load-settlement curves of an axially loaded pile with two values of bottom scour width (0 and $20 \times D$) and varying scour depths. The slope angle was taken as 40°.

The observations from the results shown in Fig. 18 are as follows. First, as scour depth increased, the estimated pile settlement in clay increased. The impact of scour depth was significant, as seen in the increase in pile head displacement as scour depth increases from 1 to 3 m. Second, the scour width had a significant impact on the axial behavior of the pile in clay. Changing the scour width from 0 to $20 \times D$, the load-settlement curves with soil effect significantly increased, especially for the curve for the 3-m scour depth, due to the reduced impact from scour hole dimensions. As discussed previously, scour hole dimensions provided additional vertical stress, which gave rise to the change in the value of ψ as shown in Eq. (8*c*) along with the effect of local scour on the remaining properties of the soil. As a result, the scour hole dimensions affected the value of the dimensionless factor (α) and undrained shear strength due to the different stress state shown in Eqs. (8*a*), (8*b*), and (9).

In addition, from Fig. 18, the impact of including the soil effect in estimating the vertical response of the pile increased in significance as scour depth increased. As scour depth increased, there was an increasing difference between the solid lines (i.e., with soil effect) and dashed lines (i.e., without soil effect), indicating the importance of including soil effects in the analysis, particularly for more severe scour scenarios. Finally, among the three values of scour depth shown, 3-m scour showed the most significant impact of soil stress history, reducing both skin friction and end-bearing capacities of the clay. The magnitude of the settlement depended on many factors, such as axial load. As a result, the last point of the line associated with $S_d = 3$ m and $S_w = 20 \times D$ (with s.e.) yielded the largest settlement value because of the combination of the

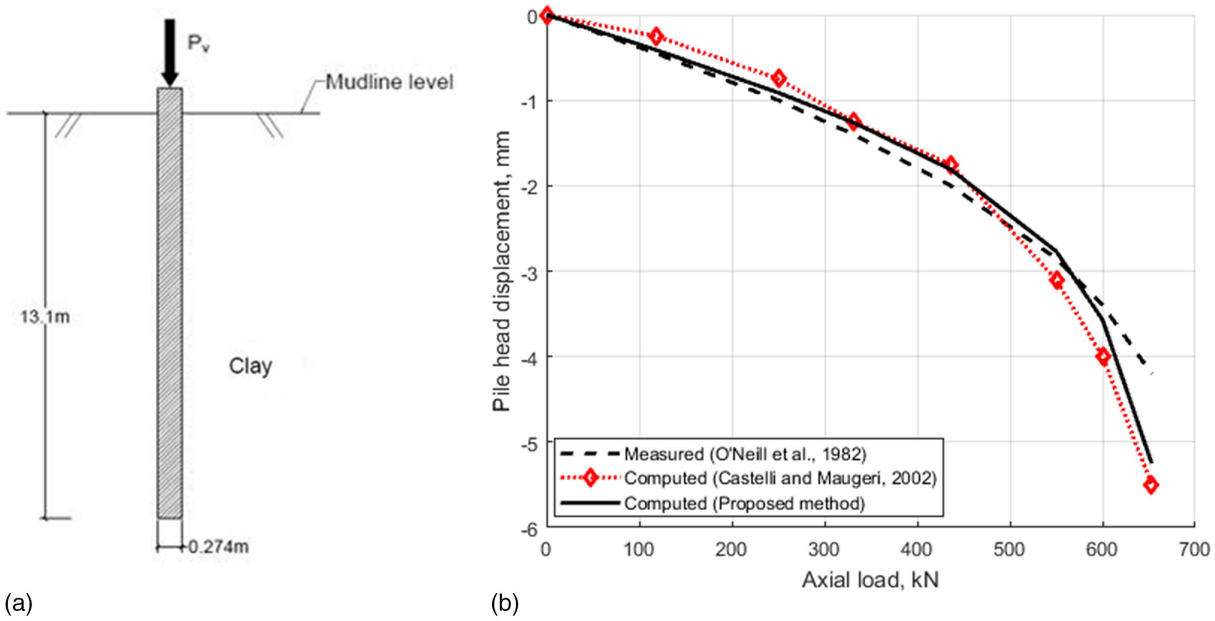

Fig. 17. (a) Axially loaded pile in clay; and (b) settlement at the pile head versus axially applied load for measured data compared with proposed model result without considering scour.

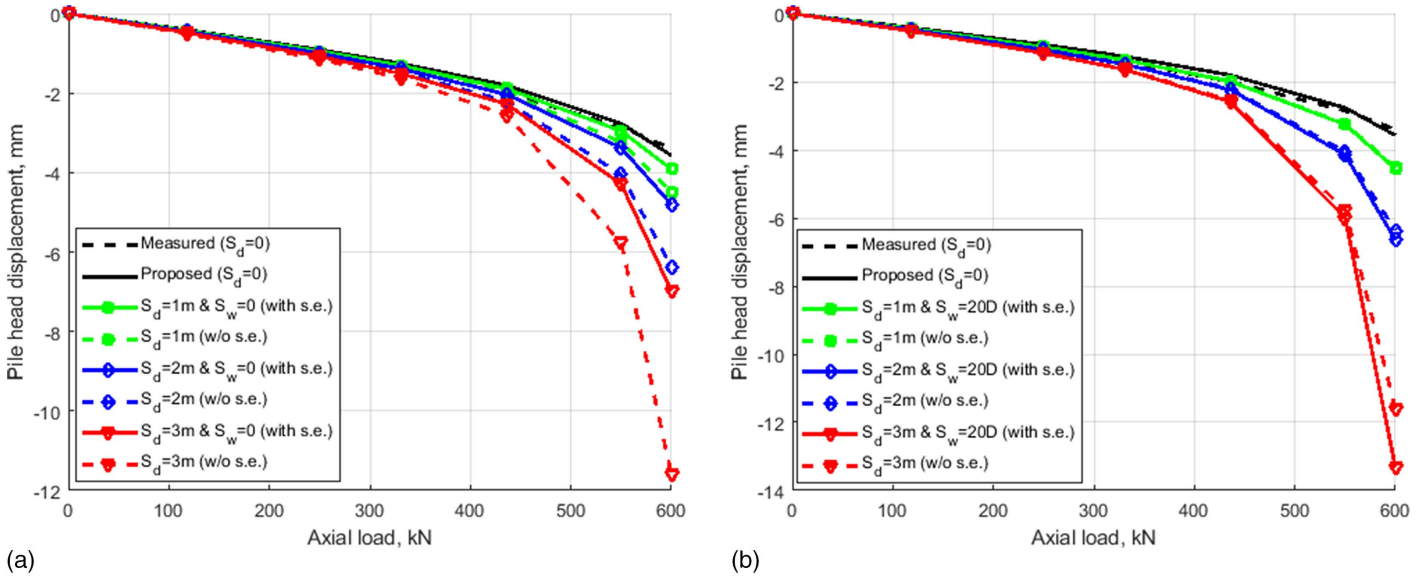

Fig. 18. Load-settlement curves at the pile head with varying scour depths and values of (a) 0; and (b) $20 \times D$ for bottom scour width in clay.

largest axial load and scour depth. In comparison, the line associated with $S_d = 3$ m (w/o s.e.) ignored the impact from stress history, which led to a relatively larger vertical resistance of the clay.

To further investigate the effect of scour width, Fig. 19 provides load-settlement curves for varying scour widths ranging from 0 to ∞ under 1- and 2-m scour depths. An infinite scour width indicates the exclusion of the effect of scour hole dimensions. Scour widths of 0 and ∞ provide upper and lower bounds for the load-settlement responses. From Fig. 19, comparing $S_d = 2$ m (w/o s.e.) and $S_d = 2$ m with $S_w = 0$ (with s.e.), the latter yielded a smaller settlement value because the effect of scour hole dimensions was the dominating factor. In other words, the reduction due to soil stress history was compensated for and overcome by the impact from scour hole dimensions with a bottom scour width of zero and slope angle of 40°. In comparison, between $S_d = 2$ m (w/o s.e.) and $S_d = 2$ m with $S_w = \infty$ (with s.e.), the latter neglected the impact of the scour hole dimensions and only considered the impact of stress history. In this case, the stress history effect diminished both frictional resistance and end-bearing resistance, as shown in Eqs. (7) and (9), due to the reduction of undrained shear strength.

To provide a more detailed view of the impact of soil stress history, Appendix II provides the calculated soil properties and ultimate soil resistances, including effective unit weight, undrained shear strength, OCR, dimensionless factor (α), skin-friction resistance, and end-bearing resistance, considering $S_d = 2$ m and $S_w = \infty$ with and without accounting for the stress history effect. The effective unit weight before considering scour is 10 kN/m^3.

Table 10 summarizes the settlement values, indicating the percentage increase in estimated settlement with and without considering the stress history effect in clay. Comparing the curve with $S_w = \infty$ and the curve without soil effect shows that the effect of stress history in clay increased settlement by as much as 61.1% for a 2-m scour depth

J. Geotech. Geoenviron. Eng., 2022, 148(5): 04022028

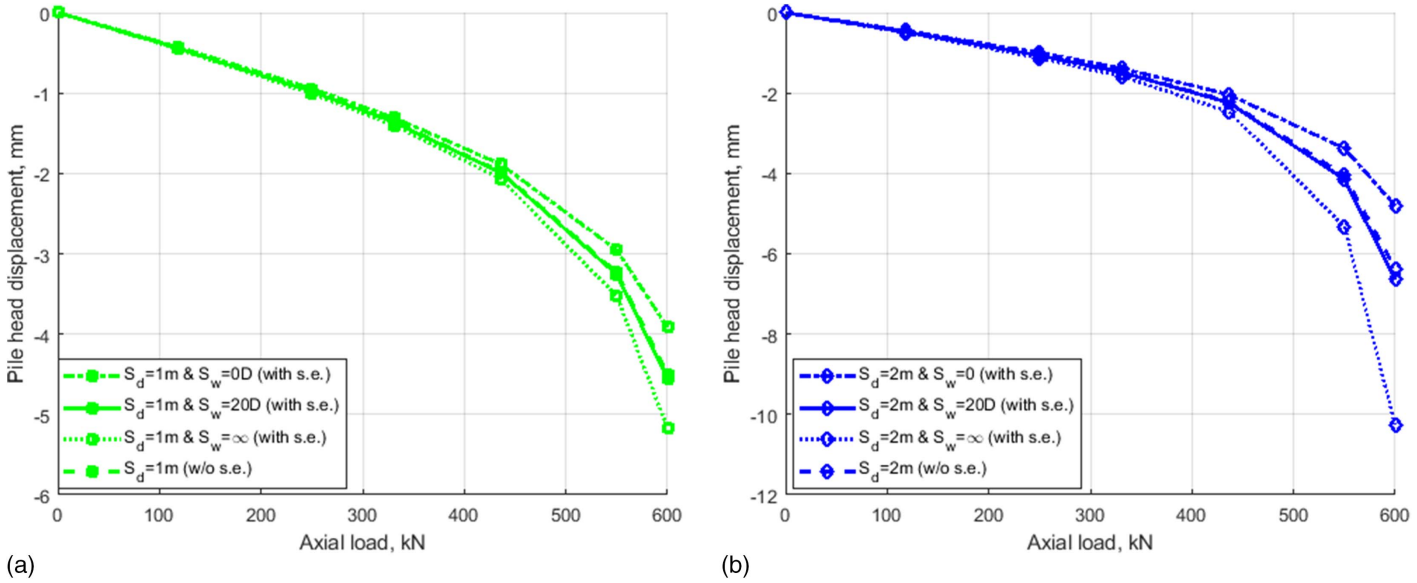

Fig. 19. Load-settlement curves at the pile head with scour depths of (a) 1 m; and (b) 2 m and varying bottom scour widths in clay.

Table 10. Summary of settlement values considering 2-m scour depth with and without including the effect of stress history in clay

Parameter	DP #1	DP #2	DP #3	DP #4	DP #5	DP #6
Axial load (kN)	118	250	331	436	550	600
Settlement without soil effect (mm)	0.47	1.05	1.47	2.21	4.05	6.37
Settlement with $S_w = \infty$ (mm)	0.50	1.12	1.59	2.46	5.33	10.26
Increase due to the effect of stress history (%)	6.1	6.7	7.7	11.4	31.5	61.1

Note: DP =data point.

and 600-kN axial load mainly due to the reduction in undrained shear strength, which led to the corresponding reductions in skin-friction resistance and end-bearing resistance. The $S_w = \infty$ case is particularly applicable to the general scour scenario where the entire mudline is lowered, or local scour cases if the bottom width of the scour hole is large. In these cases, the stress history effect dominates, leading to the most vulnerable condition for scoured bridges. The magnitude of settlement and increase of settlement depend on several factors, including scour depth, magnitude of externally applied load, length of the pile, and others.

For 1-m scour depth, as shown in Fig. 19(a), the increase of settlement was 14.8%, and the increase was 61.1% for 2-m scour depth in Fig. 19(b). The 61.1% increase in estimated settlement for clay, as well as the 34.1% increase in estimated settlement for sand found in the previous section, corresponded with the largest axial loads (600 and 311.5 kN for the clay and sand foundation, respectively), which magnified the impact of stress history. The increase in settlement values of around 3–4 mm for the current case studies were based on the loading scenarios and following the values from previous experimental tests. The proposed methodology is also applicable to other loading scenarios, including those leading to larger settlement values. In many cases, particularly more severe scour cases, neglecting to include the impact of stress history in clay leads to significant underestimation of the values of settlement under a given axial load, leading to potentially unconservative designs of axially loaded piles in clay.

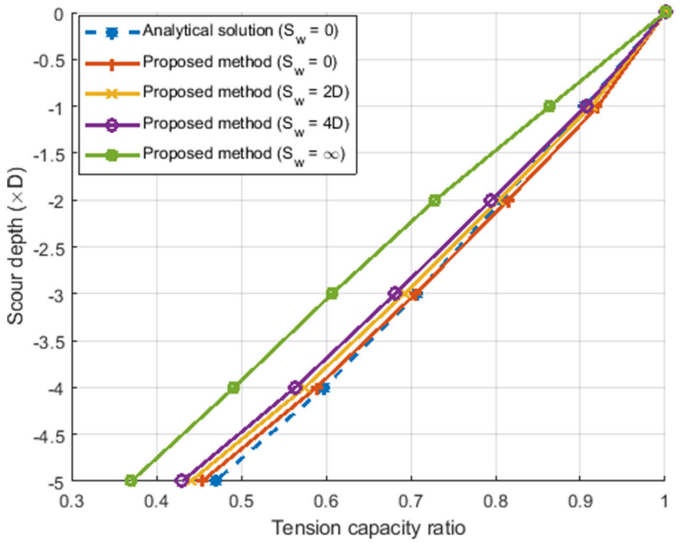

Fig. 20. Tension capacity ratios in clay with various scour depths and scour widths.

The tension capacity ratio in clay was also evaluated with the same soil profile as used for the compression test (O'Neill et al. 1982) described at the beginning of this section. Fig. 20 compares results from the proposed method with that from the analytical solution in terms of tension capacity ratio $[R_{s(\text{postscour})}/R_{s(\text{prescour})}]$ in clay. The analytical solution refers to Boussinesq's point load equation based on Lin (2017). Because previous studies have not investigated the tension capacity in clay, the analytical solution was used here for comparison, which accounts for the impact of scour hole dimensions with a closed-form expression. The proposed method refers to the method that combined both scour dimensions and soil stress history based on the proposed framework. As expected, the proposed method yielded a lower postscour tension capacity for $S_w = \infty$, mainly due to the reduction of undrained shear strength resulting from the soil stress history effect. Similar to the sand case, the increase of scour width strengthened the vertical soil resistance by providing additional stress from the scour hole dimensions. For the case with $S_w = 0$, the tension capacity

increased and even became slightly larger than the analytical solution. This is because of the following two reasons: (1) the reduction of undrained shear strength became less significant after considering the local scour effect on the properties of the remaining soil, and (2) the dimensionless factor ($\alpha_{sh\&shd}$) increased due to the reduction of ψ, as indicated in Eq. (8). Therefore, the increase of the dimensionless factor ($\alpha_{sh\&shd}$) became the governing factor, not only counteracting the reduction of undrained shear strain but also increasing the tension capacity, as shown in Eq. (10).

Conclusions

The paper presented a framework that is able to capture the impacts from both soil stress history and scour hole dimensions on the structural response of a pile for both cohesive and cohesionless soils in the presence of scour. Besides focusing on the lateral behavior of the pile, which has been investigated in the past, the proposed framework also accounted for the combined soil effects on the vertical pile behavior. The proposed framework was validated with experimental data for no-scour scenarios and verified with numerical data for scour scenarios where available for lateral and axial loadings (both tensile and compressive loadings) in sand and clay. The results from this study showed that it is essential to include both stress history and scour hole dimension effects in the modeling of soil–structure interaction in the presence of scour events. The following two points summarize the main findings from the study:

- For a sand foundation, including either the effect of stress history or scour hole dimensions could lead to a conservative design in the lateral direction. In comparison, in the vertical direction, including the effect of stress history resulted in an increase in estimated pile head deflection. For a $4 \times D$ scour depth and 311.5-kN axial load, including soil effects led to an increase in estimated settlement of 34.1%. The percentage could further increase with increasing applied axial load or increasing scour depth. These findings indicate that failing to consider soil effects under scour conditions could lead to an unconservative design, particularly under axial compressive load. Meanwhile, the impact of stress history slightly strengthened the tension capacity of the pile in sand due to the increase of soil friction angle.
- For a clay foundation, neglecting to include the effect of stress history could lead to an unconservative design in both lateral and vertical directions under scour conditions. In the lateral response of the pile in clay, the influence of stress history was the dominating factor compared with the impact of scour hole dimensions, with an increase of 13.5% in estimated lateral deflection under 3-m scour depth, $5 \times D$ scour width, and 105-kN laterally applied load. The soil effect was greater in the axial direction. Under 2-m scour depth and 600-kN axial load, the impact of including stress history effects in clay increased the estimated pile settlement by as much as 61.1% in the vertical direction in comparison with the outcome estimated without considering soil effects. An even larger percentage increase is expected if one considers higher axial load and scour depth scenarios. Likewise, the impact of stress history diminished the tension capacity of the pile in clay as a result of the reduction of undrained shear strength.

This paper provided a methodology to include soil stress history and scour hole dimension effects in the analysis of piles subject to scour in uniform soil. The potential underestimation of pile displacements under lateral and particularly axial loads if soil effects are not considered underscores the need to be able to quantitatively include soil effects in the estimation of pile responses and consider these effects for future design.

Appendix I. Calculating Changes Due to the Effect of Stress History and the Effect of Scour Hole Dimensions

Figs. 21 and 22 show the equations and overall procedures used to obtain the updated properties of sandy and clayey soils, respectively, considering the effect of stress history.

$$\phi' = \phi'_{cs} + 3D_r\left[10 - \ln\left(\frac{P'_o}{1 - \frac{2\sin(\phi')}{3 - \sin(\phi')}}\right)\right] \quad \text{(a)}$$

$$\text{Before scour: } P'_o = P'_{int} = \gamma'_{int} z_{int}\frac{3 - 2\sin(\phi')}{3} \quad \text{(b)}$$

$$\text{After scour: } P'_o = P'_{sc} = \gamma'_{int} z_{sc}\frac{3 - 2\sin(\phi')}{3} \quad \text{(c)}$$

$$OCR = \gamma'_{int} z_{\text{int}}/(\gamma'_{sc} z_{sc}) \quad \text{(d)}$$

$$\Delta D_r = \kappa \ln\left[\frac{(3 - 2\sin(\phi'))}{1 + 2(1 - \sin(\phi'))OCR^{\sin(\phi')}}\right]/(e_{max} - e_{min}) \quad \text{(e)}$$

$$D_{r\_sc} = D_{r\_int} - \Delta D_r \quad \text{(f)}$$

$$\gamma' = \frac{(G_s - 1)\gamma_w}{1 + e_{max} - D_r(e_{max} - e_{min})} \quad \text{(g)}$$

$$\Delta e = -\kappa \ln\left[\frac{1 + 2(1 - \sin(\phi'))OCR^{\sin(\phi')}}{(3 - 2\sin(\phi'))OCR}\right] \quad \text{(h)}$$

ϕ' = peak effective friction angle; ϕ'_{cs} = critical effective friction angle; P'_o = initial mean effective stress; D_r = relative density; ΔD_r = change of relative density; γ' = effective unit weight; G_s = specific gravity of soil; γ_w = unit weight of water; e_{max} = maximum void ratio; e_{max} = minimum void ratio; κ = unloading index; K_{py} = modulus of subgrade reaction; z_{int} = depth of point interest before scour; z_{sc}= depth of point interest after scour. Note that subscripts *int* indicates parameters for before and after the scour event, respectively.

Determine D_{rsc} and ΔD_r iteratively based on Eqns. (d), (e), (f), (g), and (h)

↓

Determine γ'_{sc} from Eqn.(g);
ϕ'_{sc} from Eqn. (a);
OCR from Eqn. (d);
K_{py_sc} from A.P.I. (2000) based on ϕ'_{sc}

Fig. 21. Procedures of computing soil properties considering the effect of stress history for sandy soil.

J. Geotech. Geoenviron. Eng., 2022, 148(5): 04022028

$$\gamma'_{sc} = \frac{1+e_{int}}{1+e_{sc}}\gamma'_{int} \quad \text{(a)}$$

$$e_{int} = \frac{\gamma_w + \gamma'_{int}}{\gamma_w - \gamma'_{int} w_{int}} w_{int} \quad \text{(b)}$$

$$e_{sc} = e_{int} + C_{ur}\log\left(\frac{\sigma'_{v\_int}}{\sigma'_{v\_sc}}\right) \quad \text{(c)}$$

$$\sigma'_{v\_int} = \gamma'_{int}(z_{sc} + S_d) \quad \text{(d)}$$

$$\sigma'_{v\_sc} = (\gamma'_{sc})z_{sc} \quad \text{(e)}$$

$$\gamma'_{sc} = \frac{1+e_{int}}{1+e_{int}+C_{ur}\log\left[\frac{\gamma'_{int}(z_{sc}+S_d)}{(\gamma'_{sc})z_{sc}}\right]}\gamma'_{int} \quad \text{(f)}$$

$$\frac{C_{u\_sc}/\sigma'_{v\_sc}}{C_{u\_int}/\sigma'_{v\_int}} = OCR^{\Lambda} \quad \text{(g)}$$

$$\Lambda = \frac{\lambda-\kappa}{\lambda} = 1 - \frac{C_{ur}}{C_c} \quad \text{(h)}$$

$$OCR = \frac{\gamma'_{int}(z_{sc}+S_d)}{\gamma'_{sc}z_{sc}} \quad \text{(i)}$$

γ' = effective unit weight; e = void ratio; γ_w = unit weight of water; w = soil moisture content; C_{ur} = swelling index; C_c = compression index; C_u = soil undrained shear strength; σ'_v = vertical effective stress; z_{sc} = depth of point interest after scour; λ and κ = compression and swelling indexes from isotropic consolidation tests. Note that subscripts int and sc indicate parameters for before and after the scour event, respectively.

Determine γ'_{sc} through solving Eqn. (f)

↓

Determine σ'_{v_int} & σ'_{v_sc} from Eqns. (d) and (e);
e_{sc} from Eqn. (c);
OCR from Eqn. (i);
C_{u_sc} from Eqns. (g) and (h)

Fig. 22. Procedures of computing soil properties considering the effect of stress history for clayey soil.

If $\theta < 90° - \beta$, then

$0 < z \le H_1$, $F_{ue} = F_{u0}$

$H_1 < z \le H_2$, $F_{ue} = F_{u1}$

$z > H_2$, $F_{ue} = F_{u2}$

If $\theta \ge 90° - \beta$, then

$0 < z \le H_1$, $F_{ue} = F_{u0}$

$z > H_1$, $F_{ue} = F_{u2}$

where

$$H_1 = \frac{S_w}{\tan\beta}$$

$$H_2 = \frac{S_w}{\tan\beta} + \frac{S_d}{D_1}$$

$$D_1 = \frac{\tan\beta\ \tan\theta}{1-\tan\beta\ \tan\theta}$$

F_{u0}, F_{u1}, F_{u2} and F_{ue} are given by,

$$F_{u0} = \frac{\gamma' K_o \tan\beta\, z^3}{3\cos\alpha}\left[\cos\alpha\sin\beta\tan\phi' - \sin\alpha + \frac{\tan\phi'\cos\beta}{\tan(\beta-\phi')}\right]$$

$$F_{u1} = \frac{\gamma' K_o \tan\beta}{3\cos\alpha}\left\{\left[z^3 + 3D_1\left(z^3 - \frac{z^2 S_w}{\tan\beta}\right) + 2D_1^2\left(z - \frac{S_w}{\tan\beta}\right)^3\right] \times \left[\cos\alpha\sin\beta\tan\phi' - \sin\alpha + \frac{\tan\phi'\cos\beta}{\tan(\beta-\phi')}\right]\right\}$$
$$+ \frac{1}{\tan(\beta-\phi')}\left(\frac{\gamma'(1-\tan\beta\ \tan\theta)\tan\beta}{6}\left\{3D\left[z(1+D_1) - \frac{S_w D_1}{\tan\beta}\right]^2 + 2\tan\beta\tan\alpha\left[z(1+D_1) - \frac{S_w D_1}{\tan\beta}\right]^3\right\}\right.$$
$$\left. + \frac{\gamma' S_w^2 \tan\theta}{6}(3D + 2S_w\tan\alpha)\right) - K_a\frac{\gamma' D z^2}{2}$$

$$F_{u2} = \frac{\gamma' K_o}{3\cos\alpha}\left\{\left[\left((z+S_d)\right)^3\tan\beta - 3\left(S_w - \frac{S_d}{\tan\theta}\right)S_d^2 + 2\frac{S_d^3}{\tan\theta}\right] \times \left[\cos\alpha\sin\beta\tan\phi' - \sin\alpha + \frac{\tan\phi'\cos\beta}{\tan(\beta-\phi')}\right]\right\}$$
$$+ \frac{1}{\tan(\beta-\phi')}\left\{\frac{\gamma'(z+S_d)^2\tan\beta}{6}[3D + 2(z+S_d)\tan\beta\tan\alpha] - \gamma'\frac{(S_w\tan\theta + S_d)^2}{\tan\theta}\left[\frac{D}{2} + \frac{1}{3}\left(S_w - \frac{S_d}{\tan\theta}\right)\tan\alpha\right]\right.$$
$$\left. + \gamma' S_w^2\tan\theta\left(\frac{D}{2} + \frac{S_w\tan\alpha}{3}\right)\right\} - K_a\gamma' D\frac{(z+S_d)^2 - S_d^2}{2}$$

$$F_{ue} = \frac{\gamma' K_o \tan\beta\, z_e^3}{3\cos\alpha}\left[\cos\alpha\sin\beta\tan\phi' - \sin\alpha + \frac{\tan\phi'\cos\beta}{\tan(\beta-\phi')}\right] + \frac{\gamma' z_e^2}{\tan(\beta-\phi')}\left(\frac{D\tan\beta}{2} + \frac{z_e\tan^2\beta\tan\alpha}{3}\right) - K_a\frac{\gamma' D z_e^2}{2}$$

Fig. 23. Equations used to compute the equivalent depth of interest considering the effect of scour hole dimensions for sandy soil.

Figs. 23 and 24 show the equations used to compute the equivalent depth of interest (z_e) considering scour hole dimensions for sandy and clayey soils, respectively. In Figs. 23 and 24, D_1 is the intermediate parameter, H_1 and H_2 are soil depth defining the locations of slope failure plane, F_{ue} is the ultimate soil resistance of the equivalent wedge, and F_{u0}, F_{u1}, and F_{u2} are ultimate soil resistance based on whether the slope failure plane intersects the slope of the scour hole. These procedures and equations were

J. Geotech. Geoenviron. Eng., 2022, 148(5): 04022028

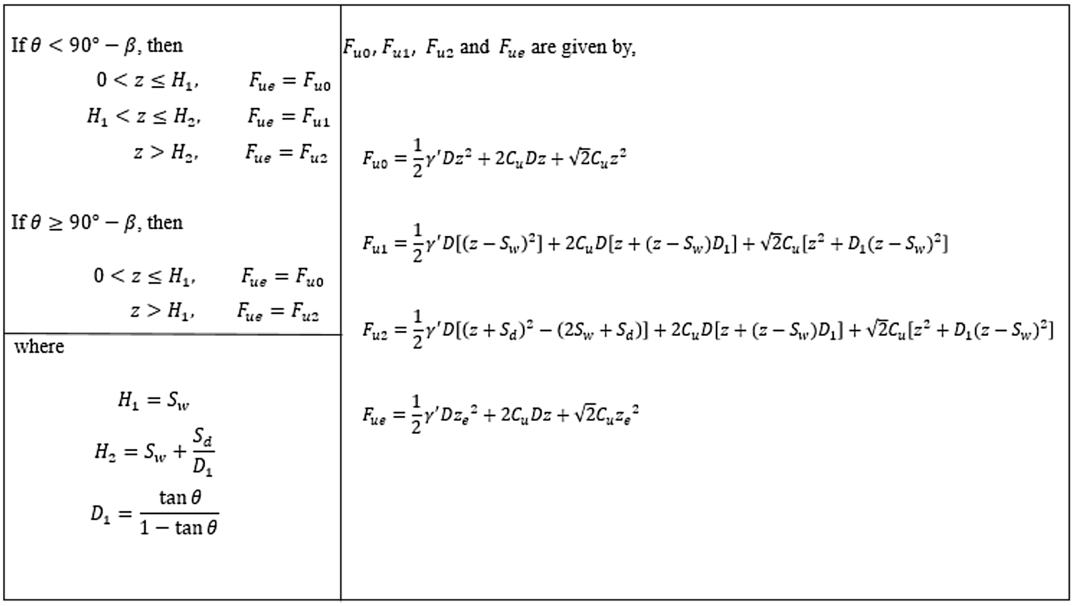

Fig. 24. Equations used to compute the equivalent depth of interest considering the effect of scour hole dimensions for clayey soil.

Table 11. Calculated soil properties and vertical ultimate soil resistances with and without considering the stress history effect for $S_d = 4 \times D$ and $S_w = \infty$ in sand with relative density 55%

z_{int} (m)	z_{sc} (m)	ϕ' (degrees)	ϕ'_{sh} (degrees)	γ'_{sh} (kN/m^3)	OCR	T_{ult} (kN/m^2)	$T_{ult(sh)}$ (kN/m^2)	Q_{ult} (kN/m^2)	$Q_{ult(sh)}$ (kN/m^2)
1.65	0.56	37.11	37.99	9.06	3.20	2.88	2.97	3,795	3,629
2.19	1.10	36.65	37.26	9.07	2.15	5.61	5.74		
2.74	1.65	36.29	36.77	9.07	1.79	8.28	8.43		
3.29	2.19	35.99	36.40	9.07	1.61	10.90	11.07		
3.83	2.74	35.75	36.10	9.08	1.51	13.49	13.67		
4.38	3.29	35.53	35.87	9.08	1.43	16.06	16.26		
4.92	3.83	35.34	35.63	9.08	1.38	18.59	18.79		
5.47	4.38	35.17	35.43	9.08	1.35	21.11	21.32	4.4% reduction in end-bearing	
6.02	4.92	35.02	35.26	9.08	1.32	23.61	23.82	resistance due to soil stress history	
6.56	5.47	34.88	35.11	9.08	1.29	26.09	26.31		
7.11	6.02	34.75	34.96	9.08	1.27	28.55	28.79		
7.65	6.56	34.63	34.83	9.08	1.26	31.01	31.25		
8.20	7.11	34.51	34.71	9.08	1.24	33.45	33.69		
8.75	7.65	34.41	34.60	9.08	1.23	35.87	36.13		
9.29	8.20	34.31	34.50	9.08	1.22	38.29	38.56		

Note: z_{int} and z_{sc} = distance between the mudline and point of interest before and after the scour event, respectively.

Table 12. Calculated soil properties and vertical ultimate soil resistances with and without considering the stress history effect for $S_d = 4 \times D$ and $\infty S_w = \infty$ in sand with relative density 65%

z_{int} (m)	z_{sc} (m)	ϕ' (degrees)	ϕ'_{sh} (degrees)	γ'_{sh} (kN/m^3)	OCR	T_{ult} (kN/m^2)	$T_{ult(sh)}$ (kN/m^2)	Q_{ult} (kN/m^2)	$Q_{ult(sh)}$ (kN/m^2)
1.65	0.56	39.16	40.24	9.26	3.13	3.10	3.22	4,736	4,616
2.19	1.10	38.62	39.36	9.28	2.10	6.02	6.18		
2.74	1.65	38.20	38.77	9.28	1.75	8.87	9.06		
3.29	2.19	37.85	38.33	9.29	1.58	11.67	11.87		
3.83	2.74	37.56	37.97	9.29	1.47	14.42	14.63		
4.38	3.29	37.31	37.67	9.29	1.40	17.13	17.36		
4.92	3.83	37.08	37.43	9.29	1.35	19.82	20.07		
5.47	4.38	36.88	37.20	9.29	1.31	22.48	22.74	2.6% reduction in end-bearing	
6.02	4.92	36.70	36.98	9.29	1.29	25.12	25.37	resistance due to soil stress history	
6.56	5.47	36.54	36.80	9.29	1.26	27.74	28.00		
7.11	6.02	36.39	36.63	9.29	1.24	30.33	30.60		
7.65	6.56	36.25	36.48	9.29	1.23	32.92	33.19		
8.20	7.11	36.12	36.33	9.29	1.21	35.49	35.77		
8.75	7.65	35.99	36.20	9.29	1.20	38.04	38.33		
9.29	8.20	35.88	36.08	9.29	1.19	40.58	40.88		

Note: z_{int} and z_{sc} = distance between the mudline and point of interest before and after the scour event, respectively.

Table 13. Calculated soil properties and vertical ultimate soil resistances with and without considering the stress history effect for $S_d = 2$ m and $S_w = \infty$ in clay

z_{int} (m)	z_{sc} (m)	γ'_{sh} (kN/m^3)	C_u (kN/m2)	$C_{u(sh)}$ (kN/m2)	OCR	α_{sh}	T_{ult} (kN/m^2)	$T_{ult(sh)}$ (kN/m^2)	Q_{ult} (kN/m^2)	$Q_{ult(sh)}$ (kN/m^2)
3	1	10.59	82.80	66.30	2.83	0.32	24.41	20.96	2,023	1,955
4	2	10.64	96.93	84.24	1.88	0.35	32.66	29.86		
5	3	10.67	111.05	100.14	1.56	0.38	40.03	37.65		
6	4	10.68	125.18	115.31	1.40	0.39	47.06	44.98		
7	5	10.69	139.30	130.13	1.31	0.40	53.91	52.09		
8	6	10.69	153.43	144.75	1.25	0.41	60.66	59.05		
9	7	10.70	167.55	159.24	1.20	0.41	67.35	65.94	3.3% reduction in end-bearing resistance due to soil stress history	
10	8	10.70	181.65	173.63	1.17	0.42	73.99	72.75		
11	9	10.71	195.78	187.98	1.14	0.42	80.60	79.53		
12	10	10.71	209.90	202.30	1.12	0.43	87.19	86.28		
13	11	10.71	224.73	217.25	1.10	0.43	93.98	93.22		

Note: z_{int} and z_{sc} = distance between the mudline and point of interest before and after the scour event, respectively.

incorporated in the framework of the proposed model presented throughout the paper.

Appendix II. Soil Properties and Vertical Ultimate Soil Resistances with and without Considering the Soil Stress History Effect

Tables 11–13 are given in this Appendix, respectively.

Data Availability Statement

All MATLAB codes and OpenSees numerical models used during the study are available from the corresponding author by request.

Acknowledgments

This project was partially funded by the INSPIRE University Transportation Center (UTC). Financial support for INSPIRE UTC projects is provided by the US Department of Transportation, Office of the Assistant Secretary for Research and Technology (USDOT/OST-R) under Grant No. 69A3551747126 through INSPIRE University Transportation Center (http://inspire-utc.mst.edu) at Missouri University of Science and Technology. The views, opinions, findings, and conclusions reflected in this publication are solely those of the authors and do not represent the official policy or position of the USDOT/OST-R, or any State or other entity.

References

API (American Petroleum Institute). 2000. *Recommended practice for planning, designing and constructing fixed offshore platforms–working stress design*. Washington, DC: API.

Boulanger, R. W., C. J. Curras, B. L. Kutter, D. W. Wilson, and A. Abghari. 1999. "Seismic soil-pile structure interaction experiments and analyses." *J. Geotech. Geoenviron. Eng.* 125 (9): 750–759. https://doi.org/10.1061/(ASCE)1090-0241(1999)125:9(750).

Briaud, J. L., L. M. Tucker, and E. Ng. 1989. "Axially loaded 5 pile group and single pile in sand." In Vol. 2 of *Proc., 12th Int. Conf. on Soil Mechanics and Foundation Engineering*, 1121–1124. London: International Society for Soil Mechanics and Geotechnical Engineering.

Castelli, F., and M. Maugeri. 2002. "Simplified nonlinear analysis for settlement prediction of pile groups." *J. Geotech. Geoenviron. Eng.* 128 (1): 76–84. https://doi.org/10.1061/(ASCE)1090-0241(2002)128:1(76).

Cox, W. R., L. C. Reese, and B. R. Grubbs. 1974. "Field testing of laterally loaded piles in sand." In *Proc., Offshore Technology Conf.* Richardson, TX: OnePetro.

Jiang, W., C. Lin, and M. Sun. 2021. "Seismic responses of monopile-supported offshore wind turbines in soft clays under scoured conditions." *Soil Dyn. Earthquake Eng.* 142 (Mar): 106549. https://doi.org/10.1016/j.soildyn.2020.106549.

Kulhawy, F. H., and P. W. Mayne. 1990. *Manual on estimating soil properties for foundation design*. Rep. No. EPRI-EL-6800. Ithaca, NY: Cornell Univ.

Lagasse, P. F., P. E. Clopper, L. W. Zevenbergen, and L. W. Girard. 2007. *Countermeasures to protect bridge piers from scour*. NCHRP Rep. No. 593. Washington, DC: Transportation Research Board.

Liang, F., X. Liang, H. Zhang, and C. Wang. 2020. "Seismic response from centrifuge model tests of a scoured bridge with a pile-group foundation." *J. Bridge Eng.* 25 (8): 04020054. https://doi.org/10.1061/(ASCE)BE.1943-5592.0001594.

Liang, F., H. Zhang, and S. Chen. 2018. "Effect of vertical load on the lateral response of offshore piles considering scour-hole geometry and stress history in marine clay." *Ocean Eng.* 158 (Jun): 64–77. https://doi.org/10.1016/j.oceaneng.2018.03.070.

Liang, F., H. Zhang, and M. Huang. 2015. "Extreme scour effects on the buckling of bridge piles considering the stress history of soft clay." *Nat. Hazard.* 77 (2): 1143–1159. https://doi.org/10.1007/s11069-015-1647-4.

Lin, C. 2017. "The loss of pile axial capacities due to scour: Vertical stress distribution." In *Proc., Int. Conf. on Transportation Infrastructure and Materials (ICTIM 2017)*. Lancaster, PA: DEStech Transactions on Materials Science and Engineering.

Lin, C., C. Bennett, J. Han, and R. L. Parsons. 2010. "Scour effects on the response of laterally loaded piles considering stress history of sand." *Comput. Geotech.* 37 (7–8): 1008–1014. https://doi.org/10.1016/j.compgeo.2010.08.009.

Lin, C., J. Han, C. Bennett, and R. L. Parsons. 2014a. "Analysis of laterally loaded piles in sand considering scour hole dimensions." *J. Geotech. Geoenviron. Eng.* 140 (6): 04014024. https://doi.org/10.1061/(ASCE)GT.1943-5606.0001111.

Lin, C., J. Han, C. Bennett, and R. L. Parsons. 2014b. "Behavior of laterally loaded piles under scour conditions considering the stress history of undrained soft clay." *J. Geotech. Geoenviron. Eng.* 140 (6): 06014005. https://doi.org/10.1061/(ASCE)GT.1943-5606.0001112.

Lin, C., J. Han, C. Bennett, and R. L. Parsons. 2014c. "Case history analysis of bridge failures due to scour." In *Climatic effects on pavement and geotechnical infrastructure*, 204–216. Reston, VA: ASCE.

Lin, C., J. Han, C. Bennett, and R. L. Parsons. 2016. "Analysis of laterally loaded piles in soft clay considering scour-hole dimensions." *Ocean Eng.* 111 (Jan): 461–470. https://doi.org/10.1016/j.oceaneng.2015.11.029.

Lin, C., and W. Jiang. 2019. "Evaluation of effective vertical stress and pile tension capacity in sands considering scour-hole dimensions." *Comput. Geotech.* 105 (Jan): 94–98. https://doi.org/10.1016/j.compgeo.2018.09.013.

Lin, Y., and C. Lin. 2020. "Scour effects on lateral behavior of pile groups in sands." *Ocean Eng.* 208 (Jul): 107420. https://doi.org/10.1016/j.oceaneng.2020.107420.

Matlock, H. 1970. "Correlation for design of laterally-loaded piles in soft clay." In *Proc., 2nd Annual Offshore Technology Conf., American Institute of Mining, Metallurgical, and Petroleum Engineers*, 277–594. Richardson, TX: OnePetro.

Mayerhof, G. G. 1976. "Bearing capacity and settlement of pile foundations." *J. Geotech. Geoenviron. Eng.* 102 (3): 197–228. https://doi.org/10.1061/AJGEB6.0000243.

McKenna, F. T. 1997. "Object-oriented finite element programming: Frameworks for analysis, algorithms and parallel computing." Doctoral dissertation, Dept. of Civil Engineering, Univ. of California.

Mosher, R. L. 1984. *Load-transfer criteria for numerical analysis of axially loaded piles in sand. Part 2. Load pile capacity curves for steel and concrete piles*. Rep. No. WES-TR-K-84-1-PT-2. Vicksburg, MS: Army Engineer Waterways Experiment Station.

O'Neill, M. W., R. A. Hawkins, and L. J. Mahar. 1982. "Load-transfer mechanisms in piles and pile groups." *J. Geotech. Eng.* 108 (12): 1605–1623.

Qi, W. G., F. P. Gao, M. F. Randolph, and B. M. Lehane. 2016. "Scour effects on p–y curves for shallowly embedded piles in sand." *Géotechnique* 66 (8): 648–660. https://doi.org/10.1680/jgeot.15.P.157.

Reese, L. C., W. R. Cox, and F. D. Koop. 1974. "Analysis of laterally loaded piles in sand." In *Proc., Offshore Technology in Civil Engineering Hall of Fame Papers from the Early Years*, 95–105.

Reese, L. C., and M. W. O'Neill. 1987. *Drilled shafts: Construction procedures and design methods.* Rep. No. FHWA-HI-88-042. Washington, DC: Federal Highway Administration.

Reese, L. C., and W. F. Van Impe. 2001. *Single pile and pile group under lateral loading I-M*. Rotterdam, Netherlands: A.A. Balkema.

Richardson, E. V., and S. R. Davis. 2001. *Evaluating scour at bridges: Hydraulic engineering circular No. 18*. Rep. No. FHWA NHI 01-001. Washington, DC: Federal Highway Administration.

Terzaghi, K. 1943. *Theoretical soil mechanics*. 11–15. New York: Wiley.

Tomlinson, M. J., and R. Boorman. 2001. *Foundation design and construction.* 7th ed. New York: Prentice Hall.

Touma, F. T., and L. C. Reese. 1974. "Behavior of bored piles in sand." *J. Geotech. Geoenviron. Eng.* 100 (7): 749–761. https://doi.org/10.1061/AJGEB6.0000065.

Vijayvergiya, V. N. 1977. "Load-movement characteristics of piles." In Vol. 2 of *Proc., 4th Symp. of Waterway, Port, Coastal and Ocean Division*, 269–284. Reston, VA: ASCE.

Wang, C., F. Liang, and X. Yu. 2017. "Experimental and numerical investigations on the performance of sacrificial piles in reducing local scour around pile groups." *Nat. Hazard.* 85 (3): 1417–1435. https://doi.org/10.1007/s11069-016-2634-0.

Wang, Z., L. Dueñas-Osorio, and J. E. Padgett. 2014. "Influence of scour effects on the seismic response of reinforced concrete bridges." *Eng. Struct.* 76 (Oct): 202–214. https://doi.org/10.1016/j.engstruct.2014.06.026.

Zhang, H., S. Chen, and F. Liang. 2016. "Effects of scour-hole dimensions and soil stress history on the behavior of laterally loaded piles in soft clay under scour conditions." *Comput. Geotech.* 84 (Apr): 198–209. https://doi.org/10.1016/j.compgeo.2016.12.008.

Zhang, H., F. Liang, and H. Zheng. 2021. "Dynamic impedance of monopiles for offshore wind turbines considering scour-hole dimensions." *Appl. Ocean Res.* 107 (Feb): 102493. https://doi.org/10.1016/j.apor.2020.102493.

Zhang, Y., and I. Tien. 2020. "Methodology to account for the impact of stress history in layered soils for seismic vulnerability assessment of scoured bridges." *Struct. Infrastruct. Eng.* 1–24. https://doi.org/10.1080/15732479.2020.1860096.